UNIVERSITY OF TARTU
Faculty of Science and Technology
Institute of Technology

Franziska Maria Bundrück

Photocatalytic degradation of 2,4-Dichloro-phenoxyacetic acid by $Cu_2Fe_{2-x}O_3/TiO_2$

Bachelor's Thesis (12 ECTS)

Curriculum Science and Technology

Supervisors:

MSc Dmytro Danilian
Assoc. Prof., PhD Rainer Pärna

Tartu 2023

Photocatalytic degradation of 2,4-Dichlorophenoxyacetic acid by $Cu_2Fe_{2-x}O_3$-TiO_2

Abstract:

As a result of human activity, large volumes of pollutants are released into the environment each year. Pesticides are widely used in agriculture and are one class of problematic compounds. There are growing concerns over public health due to the high toxicity of some of the pesticides.

A promising and affordable way to degrade pollutants in water is to use photocatalysis. However, it is problematic to remove photocatalysts from treated water. Thus, it is of pivot importance to develop reusable and easily extractable photocatalysts.

In this BSc thesis, photocatalyst based on mixture of TiO_2 and $Cu_xFe_{2-x}O_3$ was synthesized. The photocatalyst was characterized using x-ray photoelectron spectroscopy, x-ray absorption spectroscopy, scanning electron microscopy, Raman spectroscopy and UV-VIS spectroscopy. Furthermore, the performance of synthesized material was tested by measuring photocatalytic degradation of standard contaminant methylene blue and herbicide 2,4-D Under UV-A light.

The results of this study will contribute to the development of technologies for degrading hazardous pesticides.

Keywords:

Photocatalysis; herbicide 2,4 D; photoelectron spectroscopy; UV-Vis spectroscopy.

CERCS:

T150 Material technology; T155 Coatings and surface treatment

2,4-diklorofenoksüetaanhape fotokatalüütiline lagundamine kasutades $Cu_xFe_{2-x}O_3$-TiO_2 fotokatalüsaatori

Lühikokkuvõte:

Inimtegevus põhjustab pidevalt suurenevat mürkainete vabanemist keskkonda. Probleemsete ainete hulka kuuluvad ka põllumajanduses laialdaselt kasutatavad pestitsiidid. Tulenevalt mõningate pestitsiidide kõrgest toksilisusest on kerkinud päevakorda küsimus nende mõjust elanikkonna üldisele tervisele.

Üks perspektiivne ja loodussõbralik viis vee pestitsiididest puhastamiseks on kasutada fotokatalüüsi. Fotokatalüüsaatori kasutamist piirab nende puhastatud veest eraldamine. Seetõttu on oluline arendada fotokatalüsaatoreid, mida on lihtne veest eraldada ja uuesti kasutada.

Käesolevas bakalaureusetöös sünteesiti TiO_2 ja $Cu_xFe_{2-x}O_3$ segul põhinev fotokatalüsaator. Fotokatalüsaatorit iseloomustati röntgenfotoelektronspektroskoopia, röntgenkiirguse neeldumise spektroskoopia, skaneeriva elektronmikroskoopia, Ramani spektroskoopia ja UV-VIS spektroskoopia abil. Lisaks testiti sünteesitud materjali toimivust standardse saasteaine metüleen sinine ja 2,4 D lagundamisele UVA valguse toimel.

Uurimistulemused aitavad kaasa efektiivsemate mürkainete lagundamise tehnoloogiate välja töötamisele.

Võtmesõnad:

Fotokatalüüs; herbiksiid 2,4 D; fotoelektronspektroskoopia; UV-Vis spektroskoopia.

CERCS:

T150 Materjalitehnoloogia; T155 Pinded ja pinnatehnoloogia

TABLE OF CONTENTS

TERMS, ABBREVIATIONS AND NOTATIONS

2,4-D - 2,4-Dichlorophenoxyacetic acid

MB – Methylene blue

NEXAFS - Near edge X-ray absorption fine structure

SEM – Scanning electron microscope

TEY – Total electron yield

TOF-MS – Time-of-flight mass spectrometry

UHV – Ultrahigh vacuum

UVA – Ultraviolet A radiation

UV-Vis spectroscopy – spectroscopy with light in the Ultraviolet-visible range

XRD – X-ray Diffraction

XPS – X-ray Photoelectron Spectroscopy

INTRODUCTION

Pesticides are known to been used in agriculture. The chemical compounds control pests and increase the yield of crops on fields. Nowadays globally more than 2 million tonnes of pesticides are used annually (Sharma, et al. 2019). Majority of pesticides residue can affect wildlife, like grey partridges and the development of their offspring (Gaffard, et al. 2022) In humans, disorder in neurobehavioral performances can be caused by pesticides as seen in workers in the Indonesian agricultural sector (Pawestri and Sulistyaningsih 2021).

Pesticides can accumulate in nature and reach surface waters due to repeated applications on soil, spill or disposal (Syafrudin, et al. 2021). Agricultural wastewater, from e.g., tomato and potato farms, contain pesticides even after various treatments, like filtration and reverse osmosis (Sayed, et al. 2021). This shows that some wastewater treatments currently used are not effective enough to remove pesticides. The difficulties to expect are caused by different chemical and physical properties of pesticides and can most likely only be solved with a combination of various treatments (Saleh, Zouari and Al-Ghouti 2020).

One promising treatment for organic compounds is photocatalysis, where light (UV or sunlight) and photoactive catalysts are used to carry out or to accelerate chemical transformations (Anadan, Ikuma and Niwa 2010). Photocatalytic oxidation has the advantage over other treatment techniques, since it facilitates the decomposition of pollutants into simple inorganic species such as H_2O, CO_2, NO_3^-, halide ions, or more (Xu, et al. 2022). Among all kinds of photocatalysts, TiO_2 has been widely used in environmental remediation.

Following are several requirements for a good photocatalyst such as it should have a wide wavelength-range light response, good chemical stability, excellent photocatalytic performance, low cost and it should be easily removable from treated water solutions ((Xu, et al. 2022); (Belessiotis, et al. 2022)). It is also important that photocatalyst can be easily synthesized by employing a sustainable approach through a green facile route using abundant elements rather than poisonous or precious (Lashgari 2021).

One class of such materials are the spinel ferrites which have remarkable magnetic, catalytic, optical, and electrical properties (Yadav 2016). Among spinel ferrites, $CuFe_2O_4$ has received great attention as its magnetic properties can be tuned by cation distribution at octahedral and tetrahedral sites (Yadav 2016). Furthermore, by combining $CuFe_2O_4$ with TiO_2 the enhancement of visible light response, the photocatalytic efficiency and magnetically collectability can be obtained.

In this work $Cu_xFe_{2-x}O_3$ was synthesized by using a coprecipitation method. Synthesized $Cu_xFe_{2-x}O_3$ was combined with TiO_2 to obtain a photocatalytic powder. Further explanations are provided in this thesis. The material obtained was characterized by various methods. A photocatalytic evaluation has been conducted with the help of MB and in relation to an aqueous 2,4-D solution. The results of the experiments are later in this thesis discussed.

The author's contribution to this work was preparation of samples, XPS and NEXAFS measurements, SEM measurements, participation in Raman measurements, UV-Vis measurements, photocatalytic degradation of 2,4-D, data processing and analysis of results.

1 LITERATURE REVIEW

1.1 Material under study

1.1.1 Pesticide 2,4-D

One herbicide used since 1944 is 2,4-D (2,4-Dichlorophenoxyacetic acid). 2,4-D is widely used to remove broadleaf weeds from in grain, corn and grassland (Lee, et al. 2015). It is a synthetic herbicide, and it does not occur naturally in the environment.

The molar mass of 2,4-D is 221 g/mol (**Figure 1**) and its ionization energy (energy needed to remove electron from compound and create ion) is 8.5 eV. It is an aromatic compound with 3 substitutions, which include two chlorides in para and meta position to an oxyacetic acid group (**Figure 1**).

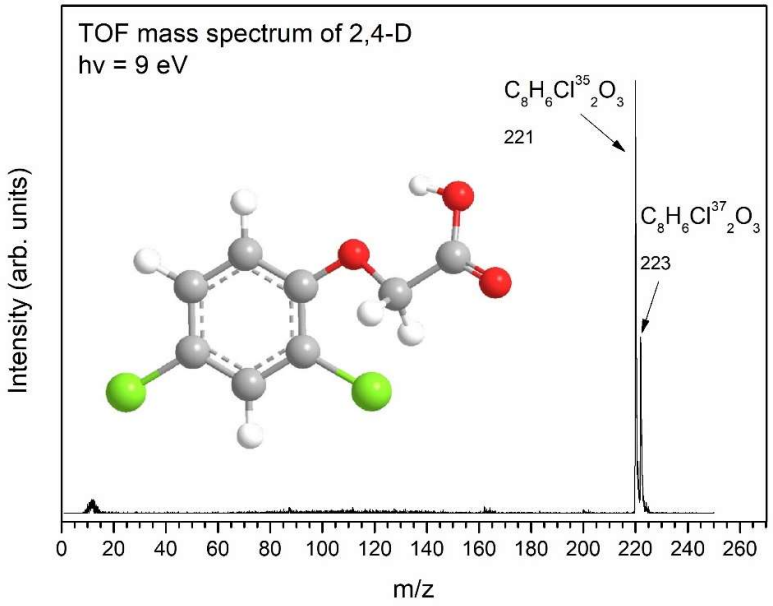

Figure 1. The TOF-MS spectra of 2,4-D was measured with excitation energy of 9 eV. The inset is the 2,4-D molecule in the ground state. Carbon atoms are marked with grey, oxygen with red, chloride with green and hydrogen with white (ACS 2012).

The half-life of 2,4-D in the environment is 10-15 days. However, it will be significantly longer when it is adsorbed silica particles, it is in cold, dry soils, or where the appropriate microbial composition is not present (ACS 2012). Thus, it is important to develop technologies which efficiently remove 2,4-D from wastewater.

1.1.2 Photocatalysis

A photocatalyst is a substance that accelerates the process of photolysis. The most common photocatalyst used is titanium dioxide (TiO_2). How TiO_2 catalysis light is described in **Figure 2**. In addition to degrading water, the electron (e^-) and hole (h^+) can also reduce and oxidise organic compounds directly. The band gap is dependent on the structure of the titania. The most common crystal structures are anatase and rutile.

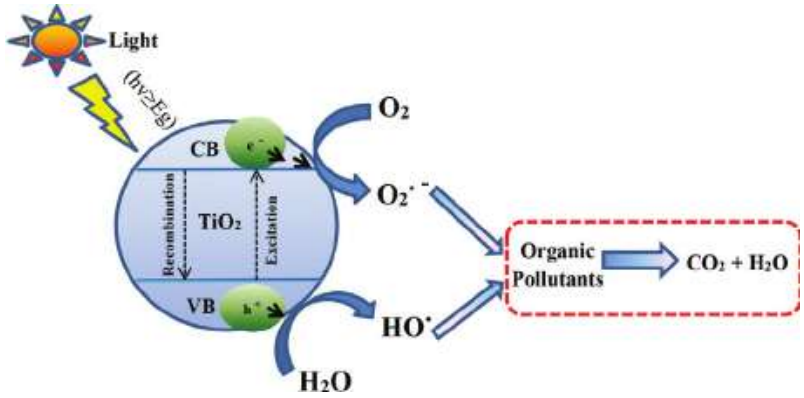

Figure 2. Illustration of processes after the absorption of light in TiO_2: Electron (e^-) at the conduction band (CB) and hole (h^+) at the valence band (VB) are generated when the photon (hv) has higher energy than the band gap (Eg). In water, the electron (e^-) then can reduce on the surface the oxygen (O_2) to O_2^-. The hole (h^+) can oxidise water (H_2O) to hydroxyl radicals (•OH). These radical species can then further degrade organic pollutants to carbon dioxide (CO_2) and water (H_2O). This figure is illustrated by (Marlina, et al. 2015).

The holes that are photogenerated at the valence band can oxidise water (H_2O) or surface hydroxyl groups (OH^-) to form hydroxyl radicals (•OH) according to the following reactions (Fujishima, Zhang and Tryk 2008):

$$TiO_2 + hv \rightarrow TiO_2 + h^+ + e^- \quad (1a)$$

$$h^+ + H_2O \rightarrow \bullet OH + h^+ \quad (1b)$$

$$h^+ + OH^- \rightarrow \bullet OH \quad (1c)$$

$$h^+ + D_{ads} \rightarrow D_{ads}^+ \quad (1d)$$

In the presence of oxygen, electrons can reduce oxygen (O_2) to produce superoxide (O_2^-) ions. Furthermore, reaction of these species can take place with protons and adsorbed H_2O to produce hydroperoxide radicals (HO_2). These radicals can then form hydrogen peroxide

(H_2O_2), which further can react the O_2 to create even more OH radicals. The following reactions can take place (Fujishima, Zhang and Tryk 2008):

$$O_2 + e^- \rightarrow \ \bullet O_2^- \tag{1e}$$

$$\bullet O_2^- + \ H^+ \rightarrow \ \bullet HO_2 \tag{1f}$$

$$2 \bullet HO_2 \rightarrow O_2 + H_2O_2 \tag{1g}$$

$$H_2O_2 + \bullet O_2^- \ \rightarrow OH^- + \ \bullet OH + O_2 \tag{1h}$$

All species, H_2O_2, O_2^-, HO_2 and •OH, that can be formed after photoabsorption by reduction and oxidation on surfaces are highly reactive. Further, this can oxidise a large variety of organic compounds.

As TiO_2 has a relatively wide band gap (3.0, rutile to 3.2 eV, anatase) it cannot be used with less intense light. Therefore, it might be improved by addition of metals or their oxides, like Cu and CuO_2, which can create a heterojunction between the bands of TiO_2 and reduce the energy gap (Janczarek and Kowalska 2017).

1.2 Characterisation techniques

1.2.1 X-ray photoelectron spectroscopy (XPS)

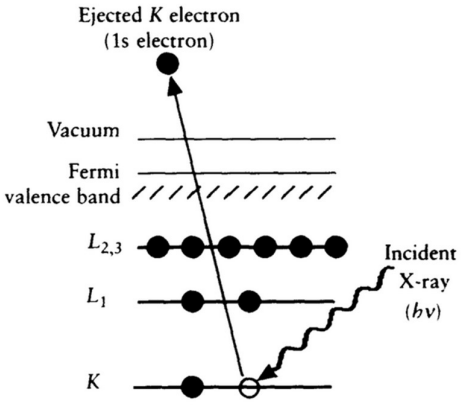

Figure 3. Schematics of the photoelectric effect during XPS. A 1s electron is ejected by an incident X-ray from its energy shell. Illustration by (Watts and Wolstenholme 2003).

XPS, also known as Electron Spectroscopy for Chemical Analysis, is a surface analysis of materials. It uses X-ray photons to bombard a sample and measures the emitted electrons.

The principle is based on the photoelectric effect. It describes an electron being ejected by a photon from an inner shell (**Figure 3**).

The energy of the emitted electrons can be detected and contains information about the binding energies of the sample substances' surface. The relation can be expressed as:

$$E_{kin} = hv - E_b, \tag{2}$$

Where E_{kin} is the kinetic energy of the emitted electron, hv is the photon energy and E_b is the binding energy. Every atom has a characteristic photoelectron spectrum. This can be used for quantitative studies of elements and their electronic state as there are unique structures and in addition it shows information on the composition in the sample (Moulder, et al. 1992).

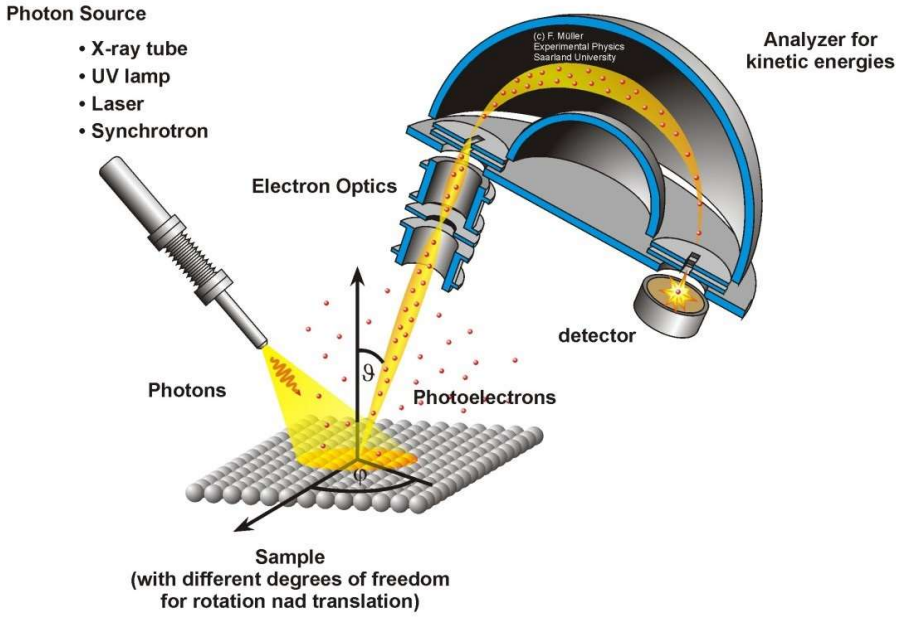

Figure 4. Principles and Parts of XPS instrumentation (Müeller 2017).

The XPS instrument (**Figure 4**) collects the emitted electrons through an optical system into the entrance slit of the analyser. Most analysers are electron energy analysers. There the electrons are directed into a hemispherical flight path by an electrical field. This allows the detector to detect the electrons at different kinetic energies, which can be converted to the binding energy.

XPS is overall an excellent technique to identify elements in the surface layer and their valence state since all elements have their core levels at specific energies.

In addition, the XPS spectra show other structures like line Auger structures and satellites. The Auger structures are created after photoionization process due to relaxation of atom by

filling the core hole with an electron from the upper energy level simultaneously by the ejection of another electron, which is called Auger effect (Watts and Wolstenholme 2003).

1.2.2 Near Edge X-ray Absorption Fine Structure Spectroscopy (NEXAFS)

This method is known as near edge X-ray absorption fine structure or X-ray absorption near-edge structure (XANES). The measurable physical quantity is an X-ray absorption coefficient. It describes how strongly X-ray photons are absorbed as a function of X-ray photon energy.

In comparison to XPS, where kinetic energy of emitted electrons are measured, in NEXAFS the emitted photoelectrons, the emitted Auger electrons and scattered emitted electrons or the sample drain current, or the emitted fluorescent photons can be measured.

The measurements of electrons can take place in different modes: total electron yield (TEY), partial electron yield (PEY) and Auger electron yield (AEY) mode. In TEY mode, the detection of electrons with all kinds of kinetic energies occurs (Stöhr 1992). When only electrons with kinetic energies within a defined region are detected, it is called PEY mode. AEY mode, a particular case of PEY, is used, when the energy window is adjusted to detect only Auger electrons in a specific region (Stöhr 1992).

These measurements can describe the characteristics, like structure and electronic state, of a compound even more detailed as it describes the transitions to unoccupied orbitals.

1.2.3 Scanning electron Microscopy (SEM)

Scanning electron microscopy (SEM) is a microscopic method, that characterises the surface with the help of a focused electron beam. It detects the emission of various radiation from the surface. The most common emissions are secondary and backscattered electrons. The image can be created by detecting the various amounts of secondary electrons.

It allows a large depth of focus with which you can determine the shape and orientation of a particle (Shaw 1992). Nowadays the resolution can be up to 1 nm.

1.2.4 Raman Spectroscopy

Raman Spectroscopy is a non-destructive chemical analysis technique. Information about chemical structure, phase and polymorphy, crystallinity and molecular interactions can be obtained. It can be observed due to the interaction of light with the chemical bonds within a material.

The principle is based on inelastic scattering of photons after the laser interacts with the sample. The gain or loss of the photon energy is happening due to interaction with the vibrational and rotational modes of the molecule. This shift is also called the Raman shift. This means that the sample is illuminated with a laser beam and the changes of the scattered photons energy is then analysed.

1.2.5 UV-Vis-Spectroscopy

UV-Vis Spectroscopy is based on the absorbance of light in the UV-Vis spectrum by organic compounds. This region includes the wavelength range of 800-200 nm, which in terms of energy is 1.5-6.2 eV.

This instrumentation can be used for qualitative and quantitative analysis. As some different structures of organic molecules have unique structures, spectra are characteristic to different substances. For quantitative analysis, the Beer's Law shows a dependence between absorbance A and molar concentration c of a substance in a solution:

$$A_\lambda = log(\frac{I_0}{I}) = \varepsilon_\lambda bc, \quad (3)$$

Where I_0 is the initial intensity of light, I is the light intensity detected, ε is the molar conductivity and b is the radiation path length. As the molar conductivity ε and the radiation path length b are the same for solutions with different concentrations of the same substance measured by the same instrumentation, absorbance A is linearly dependent on the molar concentration c.

Following this concept, the degradation of an organic compound over time can be observed via UV-Vis spectroscopy. To measure the activity of the photocatalyst, this thesis uses MB (methylene blue) as the compound to be degraded. MB has a characteristic absorption between 550nm and 750nm.

Another UV-Vis spectroscopy technique, used in this thesis, is diffuse reflectance spectroscopy. This method is based on the scattering of light in several directions on mostly rough surfaces. The light is directed onto the sample and then transmittance and reflectance can be detected. The optical properties and structures of solid materials, especially powdered samples, can be characterised by this absorbance technique. An important property for photocatalyst measured with this method is the band gap width.

2 THE AIMS OF THE THESIS

The aims of the thesis are following:

- Our goal was to synthesize photocatalyst for water purification from contaminates such as pesticides, which is recoverable.
- The purpose of this work was to develop a simple synthesis method for $Cu_xFe_{2-x}O_3$ - TiO_2, where TiO_2 is attached to surface of synthesized $Cu_xFe_{2-x}O_3$.
- We aimed to enhance the visible light response of synthesized photocatalyst and to maintain photocatalytic activity.
- We focused on this work to prepare material which is easy to capture from water.

3 EXPERIMENTAL PART

MATERIALS AND METHODS

3.1 Material under investigation

3.1.1 Materials and Equipment

3.1.1.1 Chemicals used in thesis

The reactants for synthesis of photocatalyst were obtained from Sigma Aldrich. The $Cu(NO_3)_2$ x $3H_2O$ was 99 % in purity (trace metal based), the $Fe(NO_3)_3$ x $9H_2O$ was 99 % purity (trace metal based), and NH_4OH was 98 % in purity. For synthesis 2.24 M solution of NH_4OH was prepared (150 ml deionised water and 50 ml 25% NH_4OH). The TiO_2 used is synthesis was P25 obtained from Sigma Aldrich 99% in purity (trace metal based). The de-ionized water was obtained from reverse osmosis water purification device (Bernstead, Pacific TII). In order to fix photocatalyst on the surface, we used 99.99% pure Indium.

The 2,4 D (also shown on **Figure 1**) had purity of 98% (pestinal grade) and was purchased from Alfa Aesar GmbH Co KG, Germany.

The photocatalytic evaluation of our material was performed by degrading 10^{-5} M MB and 10^{-5} M 2,4 D in water.

3.1.1.2 Basic laboratory equipment used

We used the following laboratory equipment: (i) Analytical laboratory scale KERN ALS 220-4N (max 220g, d = 0,1 mg), (ii) Magnetic Stir Plate IKA C-MAG HS 7, (iii) Temperature controller IKA ETS-D5, (iv) Hielscher Ultrasonic processor UP200Ht, (v) Centrifuges Thermo Scientific Heraeus Multifuge X1R, (vi) Oven Nabertherm P330 (30 - 3000 °C), (vii) Climate Chamber Memmert CTC 256, (viii) LED PROZEKTOR Forever Light (150W, 6000K, 12000LM, IP66), (ix) UVA lamp – 4 Hg fluorescent light bulbs (15 W, iSOLde Cleo, λ_{max} = 355nm)

3.1.2 Preparation of photocatalyst $Cu_xFe_{2-x}O_3$-TiO_2

3.1.2.1 Preparation method 1 (PM1)

This method of synthesis was adapted by Dmytro Danilian. Firstly, $Cu_xFe_{2-x}O_3$ is synthesised by coprecipitation. For this, $Cu(NO_3)_2$ x $3H_2O$ (0.01 mol) and $Fe(NO_3)_3$ x $9H_2O$ (0.02 mol)

are dissolved in 150 ml of triple-distilled water. To get a homogenous solution, it is continuously stirred at room temperature. Then a 3.34 M solution of ammonia hydroxide is added dropwise to the solution until the pH is adjusted to about 11 and precipitation is completed.

After this the solution is washed five times with deionised water using a glass pipette. Between each wash cycle the precipitant is settled down for 15 minutes and during each wash 60-70% of the total amount of liquid is discarded with avoiding the transfer of precipitants with the pipette. After final washing solution should be transparent. To separate the nanoparticles from the rest of the solution it is centrifuged at 2000 rpm for 5 minutes.

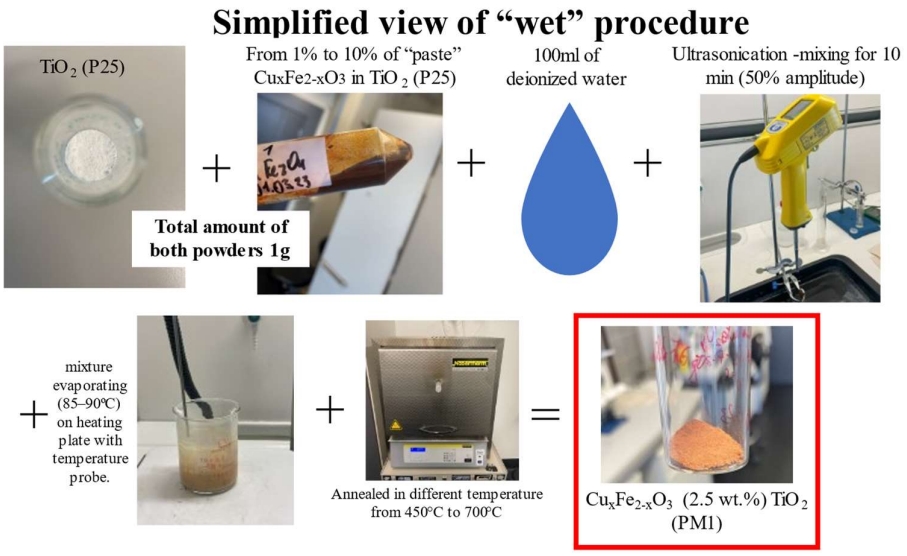

Figure 5. Description with pictures of preparation method 1 (wet method).

For the first preparation method (PM1) as seen in **Figure 5**, the washed precipitate, a wet viscous paste, is then weighted and 2.5%, 5% and 10% are taking from the total amount of suspension into separate glass beakers. To the separated pastes 0.95 g of TiO_2-P25 and 100 ml of deionised water is added. The solution is mixed by ultrasonication with 50% amplitude for 10 minutes. After that the water is evaporated by putting the solution on heating plates at 85-90°C overnight. Lastly, the precipitate is weighed and dried at 50-60 °C for 12 hours, and annealed at different temperature modes, 500°C, 600°C or 700°C, for 4 hours. Before any further measurements, the powders are grinded by mortar for 5 minutes. This method is so called "wet preparation method". Some samples prepared with this method are additionally modified with annealing them at 600°C for 24 hours.

3.1.2.2 Preparation method 2 (PM2)

For the second preparation method as seen in **Figure 6**, the washed precipitate is first dried at 50-60°C for 12 hours. After that, the powders are annealed at different temperatures, 500 and 700°C, for 4 hours. Then 20% of the synthesized powder is mixed with a mortar for 30 minutes. The mixture of powder is then annealed for 24 h at 600°C. This method is called dry or mechanical method.

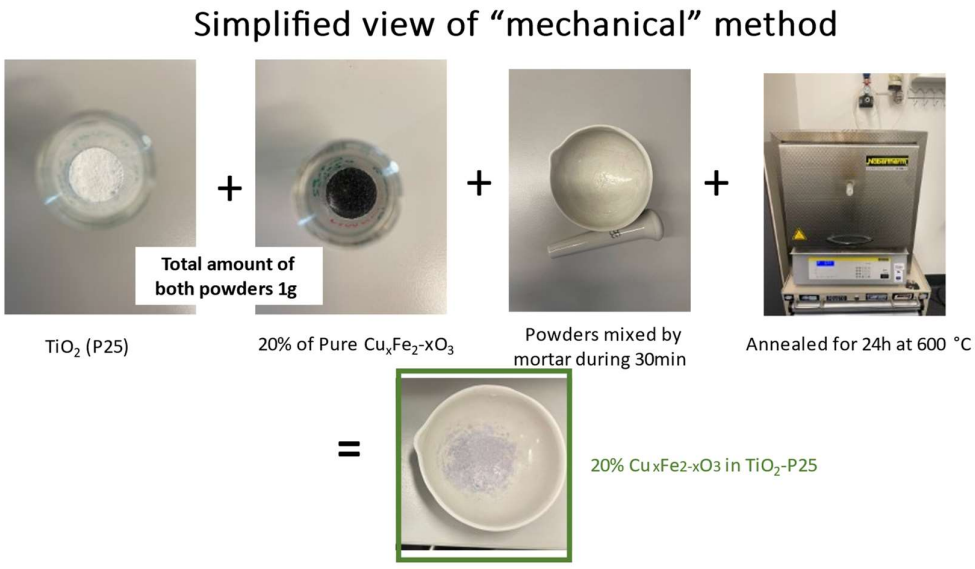

Figure 6. Description with Pictures of preparation method 2 (dry/mechanical method).

3.1.2.3 Naming of different prepared powders

In this thesis we focus on characterisation and performance of following sample prepared through PM1: $Cu_xFe_{2-x}O_3$ (2.5 wt.%) – TiO_2 (P25) annealed at 500 °C for 4 h (will be referred as $Cu_xFe_{2-x}O_3$ (2.5 wt.%) – TiO_2 (PM1) and sample prepared through PM2: $Cu_xFe_{2-x}O_3$ (20 wt. %) - TiO_2 annealed at 700 °C annealed for 24 h at 600 °C (will be referred as $Cu_xFe_{2-x}O_3$ (20 wt.%) – TiO_2 (PM2).

As pure reference material we have selected following samples: pure TiO2 (P25), pure TiO2 (P25) annealed for 24 h at 600 °C (referred as TiO2 600°C), pure synthesized $Cu_xFe_{2-x}O_3$ at 500°C (will be referred as $Cu_xFe_{2-x}O_3$ 500°C) and pure synthesized 7 $Cu_xFe_{2-x}O_3$ annealed at 700°C (will be referred as $Cu_xFe_{2-x}O_3$ 700 °C).

Other prepared samples used for comparison are following: $Cu_xFe_{2-x}O_3$ (10 wt. %) – TiO_2 annealed at 700 °C (PM 1) (will be referred as $Cu_xFe_{2-x}O_3$ (10 wt.%) – TiO_2 (PM2)), $Cu_xFe_{2-x}O_3$ (5 wt.%) – TiO_2 annealed at 700 °C (PM1) (will be referred as $Cu_xFe_{2-x}O_3$ (5 wt.%) –

TiO_2 (PM2)) and $Cu_xFe_{2-x}O_3$ (2.5 wt.%) – TiO_2 annealed at 500°C (PM1) with additional annealing of 600 for 24 hours h (will be referred as $Cu_xFe_{2-x}O_3$ (2.5 wt.%) – TiO_2 + 600 °C (PM1)**).**

3.1.2.4 Preparation of Photocatalyst for XPS and NEXAFS measurements

For preparation, the powders were pressed on copper plates with pure indium. The preparation plates are then inserted in the vacuum chamber. As a reference a golden piece is placed on an additional indium patch.

3.2 Experimental methods

3.2.1 XPS surface study

The $Cu_xFe_{2-x}O_3$-TiO_2 XPS experiments were conducted using a surface station of the UT Physics Institute equipped with an electron energy analyzer (SCIENTA SES 100) and a non-monochromatic twin anode X-ray tube (Thermo XR3E2), with characteristic energies of 1253.6 eV (Mg $K_{a1,2}$ FWHM 0.68 eV) and 1486.6 eV (Al $K_{a1,2}$ FWHM 0.83 eV).

All XPS measurements were performed in ultrahigh vacuum (UHV) conditions ($<5x10^{-9}$ mbar). The analyzer–source angle was 45°. The binding energy scales for the XPS experiments were referenced to the binding energy of C 1s (284.8 eV) photoemission line. Raw data were processed using Casa XPS (version 2.3.16) (Fairley, et al. 2021) software. Data processing involved removal of K_a and K_b satellites and the background, and fitting of components. Background removal was done using Shirley background, for fitting components a Gauss-Lorentz hybrid function was used (GL70, Gauss 30%, Lorentz 70%) for the best fit.

The overall atomic concentrations of elements were estimated by using Average Relative Matrix Sensitivity Factors (AMRSF) (Seah, Gilmore und Spencer 2001) and our instruments transmission function. Elemental composition was estimated by Rainer Pärna. However elemental composition in Table 1 shows trends only, since XPS in very surface sensitive technique (information depth less than 3 nm).

3.2.2 NEXAFS

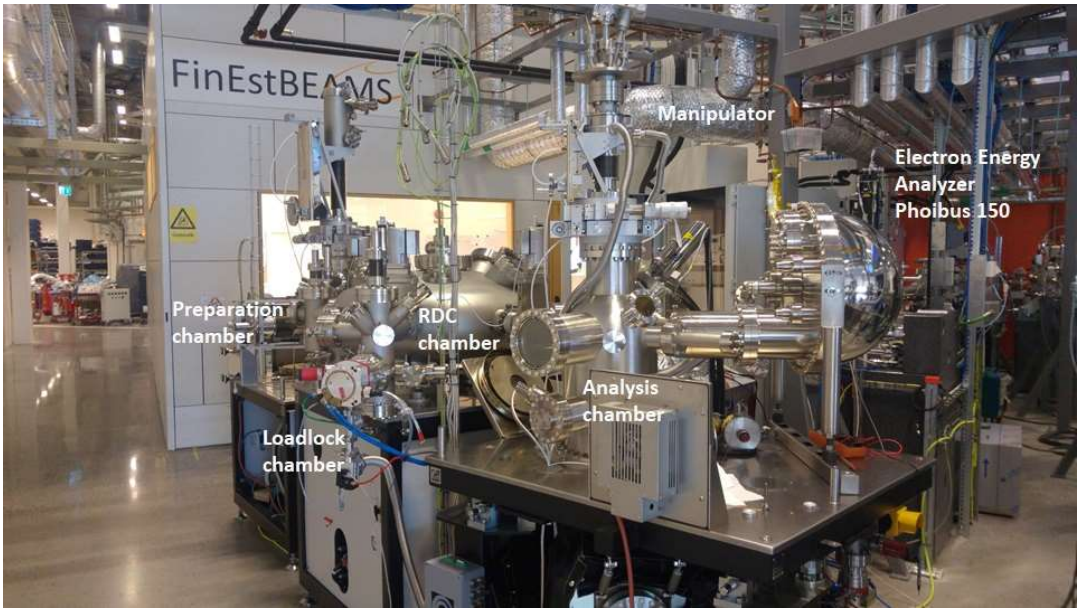

Figure 7. Set up of the Solid-state endstation of the FinEstBeams at MAX-IV synchrotron in Lund, Sweden.

The NEAXFS measurements were done at the solid-state endstation of the FinEstBeaMS at the MAX-IV synchrotron in Lund, Sweden as shown in **Figure 7**. The endstation consists of four main chambers: loadlock chamber to insert the samples, RDC chamber to move samples between experimental chamber, Preparation chamber to prepare samples with various techniques and Analysis chamber to carry out measurements.

The endstation is equipped with Phoibus 150 electron energy analyser and has capability to measure NEXAFS. The NEXAFS was measured in the total electron yield mode by measuring sample drain current. The drain current was measured by using 5–axes manipulator and ALBA electrometer developed in MAX IV laboratory.

Data processing involved removal of background simultaneously measured from the gold mesh placed in front of the sample.

3.2.3 SEM

Imaging was performed using FEI Nova NanoSEM 450 (Lincoln, NE, USA). The SEM images of the samples were taken at normal incidence with usage of an electron beam with the corresponding energy of 10 kV high voltage. The samples were prepared on carbon tape and covered with gold to minimise charging. The gold coating was done using Emitech sputter coater.

3.2.4 Raman

The Raman spectra were measured by using the Renishaw in Via Micro-Raman microscope at room temperature. The powders were put on a silicon wafer. The wavelength of the Argon laser was 514.5 nm, the spot size, the spatial resolution was 1μm and incident power 1 mW. The spectral resolution of the Raman spectrometer is estimated to be approximately 2 cm.

3.2.5 UV-Vis Absorption Spectroscopy

The evaluation of the optical absorption, optical transmission and reflection measurements of our samples were conducted with an Agilent Cary 5000 UV-Vis-NIR spectrometer equipped with a tungsten lamp and a photomultiplier. Resolution in UV-Vis region was 0.1 nm. As baseline for diffuse reflectance spectroscopy polytetrafluoroethylene (PTFE) was used.

3.2.6 Photocatalytic evaluation

3.2.6.1 Photocatalytic degradation of methylene blue as standard contaminant

For preparation 10 mg of the photocatalyst, $Cu_xFe_{2-x}O_3$-TiO_2, is put on a stainless-steel plate with 99.99% pure indium pressed on it. The indium is used to attach the photocatalytic powder uniformly and control the distribution of particles in the solution. For each powder several parallels (2-3) of 10mg each were prepared. The plates are put in Petri dishes and 10 ml of 10^{-5} M MB aqueous solution is added to each plate. The initial absorbance of MB in each plate is measured by UV-Vis spectrometer. The characteristics of MB can be found in the region between 550-750 nm. The solutions are put under the UVA light (tungsten lamp) or visible light source (LED lamp) in the climate chamber at 22.5°C with 90% humidity. To avoid the condensation of the solutions during that time, the Petri dishes were covered by borosilicate cover glasses. It was not possible to magnetically stir the solutions as the samples prepared with $CuFe_2O_4$ have magnetic properties. The set up is shown in **Figure 8**. The absorbance is then measured after certain time intervals. For these measurements, 2 ml of the solutions are measured into plastic cuvettes, which act as the sample in the instrument, and afterwards poured back into the petri dish. The cuvettes are made of plastic and allow transmission in the wavelength region used. The last measurement was done after leaving the solutions under the light source overnight for about 18 hours. The UV-Vis absorption of each sample after the exposure time is compared to the initial absorption. With the help of Origin project, the absorption is converted into the concentration of MB over time and expressed as the degradation of MB over time of light exposure.

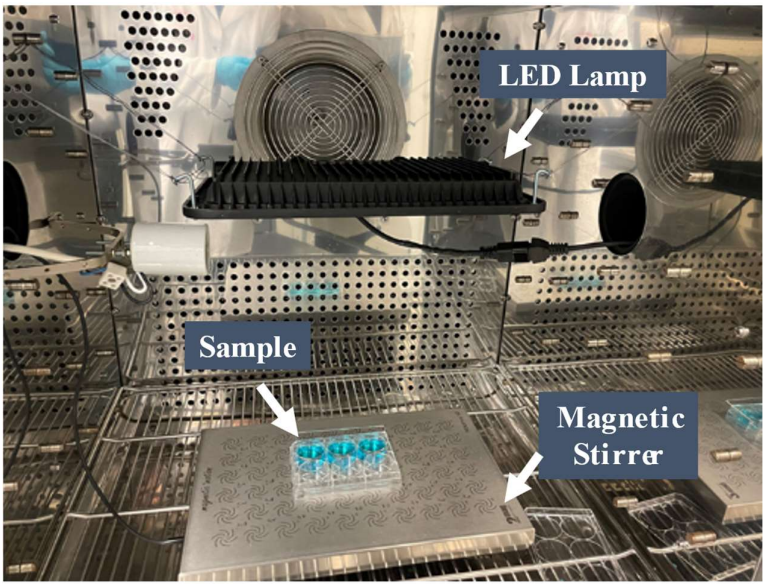

Figure 8. Picture of the photocatalytic evaluation setup in the climate chamber with the LED lamp.

3.2.6.2 Photocatalytic degradation of 2,4-D

How the degradation of 2,4-D with the photocatalyst takes place over time was similarly measured to the photocatalytic evaluation. As preparation a 10^{-5} M solution was prepared by solid 2,4-D and deionised water. The cuvettes used for these measurements are made from quartz. For every cuvette 3.5 ml of the 2,4-D solution is prepared. The powders analysed are distributed each with 3.5 mg to a cuvette to have the final concentration of 1 mg/ml. For each powder analysed one parallel was measured except for $Cu_xFe_{2-x}O_3$ (20 wt.%) – TiO_2 (PM2) which was measured in 2 parallels. After adding powder and the herbicide solution, the cuvettes are closed off airtight with a cover and plastic film. The suspensions are then put into the climate chamber at 22.5°C without light for 30 minutes before the measurements at zero hours. This is to take into consideration the adsorbance of the catalyst. The UV-Vis measurements were taken in the interval of 500-200nm. After that the suspensions were exposed to the light source for certain intervals in the climate chamber and measured in between until 21 hours.

3.3 RESULTS AND DISCUSSION

3.3.1 Material characterization

The surface elemental composition and chemical state of elements was characterized by the XPS. The overview spectrum (**Figure 9**), composition (**Table 1**), Cu 2p, Fe 2p and Ti 2p detailed spectra (**Figure 10**) are presented below.

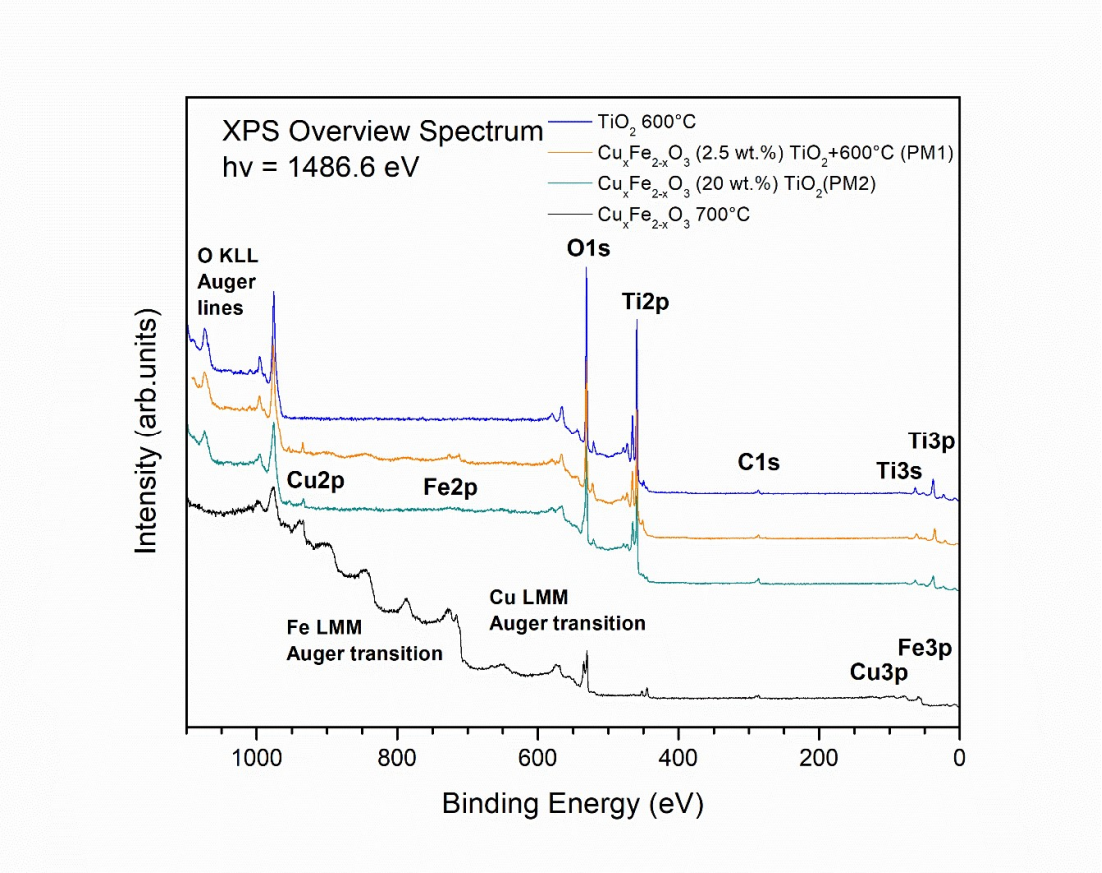

Figure 9. The overview XPS spectrum (scan step 0.5 eV) of TiO_2 600 °C, $Cu_xFe_{2-x}O_3$ (20 wt.%) – TiO_2 (PM2), $Cu_xFe_{2-x}O_3$ (2.5 wt.%) – TiO_2 + 600°C (PM1) and pure $Cu_xFe_{2-x}O_3$ annealed 4 h at 700°C.

On overview XP spectrum, the main photoelectron lines are marked as element and transition (i.e. Fe 2p) and Auger transitions as element and Auger transition type (i.e. O KLL) in overview spectrum (**Figure 9**). TiO_2 annealed at 600 °C contained Ti, O and small amount of C (3.6 atomic%, **Table 1**). The carbon is mainly residual carbon located at 284.8 eV. The synthesized $Cu_xFe_{2-x}O_3$ is composed of Cu, Fe and O. There is a difference in composition

of pure $Cu_xFe_{2-x}O_3$ annealed at 500 °C and 700 °C. The $Cu_xFe_{2-x}O_3$ 500°C contains slightly (3 atomic%) more Fe than Cu. However, the sample annealed at 700°C contained almost 10 atomic % more Fe than Cu. This can be related to higher mobility of Cu atoms, which move toward to surface when $Cu_xFe_{2-x}O_3$ is annealed at 700 °C. The synthesis was relatively clean, less than 6 atomic % of carbon is present. This carbon can be residual carbon absorbed on the surface from atmosphere (284.8 eV).

The sample $Cu_xFe_{2-x}O_3$ (2.5 wt.%) – TiO_2 + 600°C (PM1) composed of mainly from TiO_2. It had 3 atomic % of Cu and 4 atomic % of Fe present in the surface layer. However, sample $Cu_xFe_{2-x}O_3$ (20 wt.%) – TiO_2 (PM2) contained two times more Cu than Fe in the surface layer. This is related to difference in synthesis methods. Sample $Cu_xFe_{2-x}O_3$ (20 wt.%) – TiO_2 (PM2) was prepared using $Cu_xFe_{2-x}O_3$, which was initially annealed at 700 °C for 4 hours, but sample $Cu_xFe_{2-x}O_3$ (2.5 wt.%) – TiO_2 + 600°C (PM1) was annealed initially 500°C for 4 hours.

Table 1. The concentrations of Cu, Fe, Ti, O and C as atomic percent in surface region of samples (depth less than 3 nm).

	Cu	Fe	O	C	Ti
TiO_2 600°C			53	4	43
$Cu_xFe_{2-x}O_3$ (20 wt.%) – TiO_2 (PM2)	5	2	35	9	49
$Cu_xFe_{2-x}O_3$ (2.5 wt.%) – TiO_2 (PM1)	3	4	49	4	40
$Cu_xFe_{2-x}O_3$ 700°C	25	28	42	6	
$Cu_xFe_{2-x}O_3$ 500°C	21	30	45	4	

Figure 10 displays the detailed XP spectra of Cu 2p, Fe 2p and Ti 2p. In Ti 2p XP spectra, Ti $2p_{3/2}$ and $2p_{1/2}$ bands (**Figure 10 c**) are located at 458.6 eV and 464.3 eV and separated by 5.7 eV. This is in good agreement with other TiO_2 studies (McCafferty und Wightman 1998). In the Ti 2p XP spectra of all the samples only the Ti^{4+} photoemission bands were observed. Although Ti 2p spectra of the sample $Cu_xFe_{2-x}O_3$ (2.5 wt.%) – TiO_2 + 600°C (PM1) had a small shoulder at lower binding energy. This is due to indium. Indium was used to fix sample on the measurement plate.

The Fe 2p photoelectron spectra of samples **(Figure 10 b)** were complicated to analyse since presence of Cu LMM auger line under Fe2p. The Fe $2p_{3/2}$ photoelectron peak positions at 710.8 eV and $2p_{1/2}$ at 723.5 eV, spin-orbit splitting was 12.8 eV. Spectra exhibited also distinguishable satellite structure at 4.7 eV above main photoelectron line. From Fe 2p

XP spectra of both samples it can be concluded that iron ions in samples synthesized with PM1 and PM2 were in the 3+ oxidation state ($CuFe_2O_4$ or Fe_2O_3).

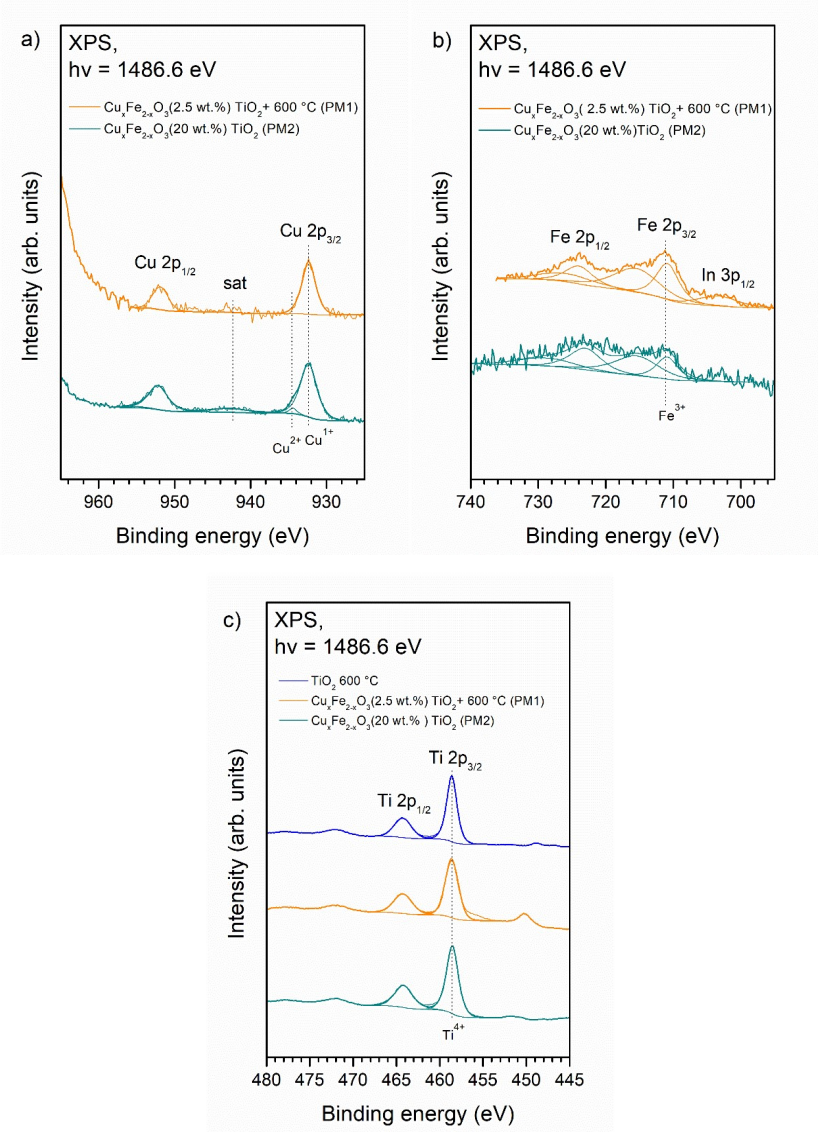

Figure 10. (**a)** Cu 2p photoelectron spectra (scan step 0.05 eV), (**b)** Fe 2p photoelectron spectra (scan step 0.05 eV) and (**c)** Ti 2p photoelectron spectra (scan step 0.05 eV) of $Cu_xFe_{2-x}O_3$ (20 wt.%) – TiO_2 (PM2), $Cu_xFe_{2-x}O_3$ (2.5 wt.%) – TiO_2 + 600°C (PM1) and pure TiO_2

The Cu 2p photoelectron spectra of samples are displayed on **Figure 10 a.** The observed photoelectron lines at 932.5 eV and 953 eV and are typical for Cu^{1+} compound (Moulder, et al. 1992). However, small amount of Cu^{1+} transforms into Cu^{2+} during annealing at 700 °C small shoulder and satellite appears in Cu $2p_{3/2}$ photo-line. This is evidence of Cu^{2+} compound (an der Laan, et al. 1981).

In order to further analyse chemical state and local electronic structure of synthesized samples NEXAFS was used. The following results are from the NEXAFS studies, where the Cu and Fe L_{23} edge spectra of the synthesised samples are discussed.

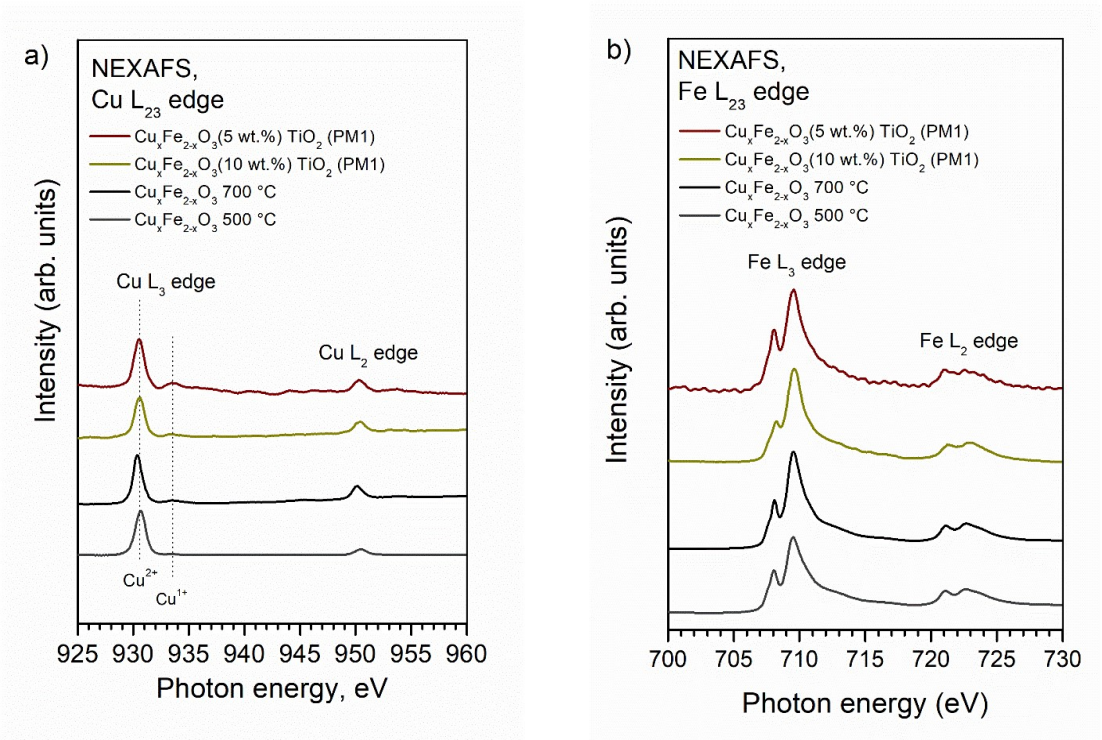

Figure 11. X-ray absorption spectra of **(a)** Cu L_{23}-edge and **(b)** Fe L_{23}-edge of $CuFe_2O_4$ (10 wt.%) – TiO_2 (PM1), $CuFe_2O_4$ (5 wt.%) – TiO_2 (PM1) and $CuFe_2O_4$ 700°C and 500°C.

The NEXAFS Cu L-edges from the synthesised and prepared powders can be seen at 930.5 eV, 933.5 eV and 950.2 eV (**Figure 11 a**). According to (Grioni, et al. 1989) a peak of 931 eV corresponds to the L_3-edge of Cu^{2+} and a peak of 934 eV to the L_3-edge of Cu^{1+}. Similar features can be also observed in the Cu L_2-edge. It should be noted that NEXAFS measured in TEY mode (in our case sample drain current) is more bulk sensitive than XPS (depth up to 10 nm (Stöhr 1992)). Thus, under the surface, samples contain mainly Cu^{2+}.

The NEXAFS Fe L_{23}-edges from the synthesised and prepared powders can be seen at 708 eV and at 709.5 eV and two adjacent shoulders at 721 eV and 722.5 eV (**Figure 11 b**). In accordance with (Garvie, Craven and Brydson 1994) the NEXAFS of L_3 and L_2-edges is related to Fe^{3+}. The observed NEXAFS structure of $Cu_xFe_{2-x}O_3$ annealed at 500 °C is very similar to one observed in case of hematite (α-Fe_2O_3). The observed NEXAFS structure of

$Cu_xFe_{2-x}O_3$ annealed at 700 °C is mostly related to hematite with addition of maghemite (fingerprint is difference in hight of pre-edge at 708 eV and edge at 709.5 eV feature compared to hematite). (Michelin, et al. 2013). The sample $Cu_xFe_{2-x}O_3$ (10 wt.%) – TiO_2 (PM1) has clearly similar structure to maghemite (γ-Fe_2O_3) (Michelin, et al. 2013). Maghemite has a spinel structure that is similar to that of magnetite but with vacancies in the cation sublattice.

In the following paragraph, Raman spectroscopy was used to analyse the phase composition of samples.

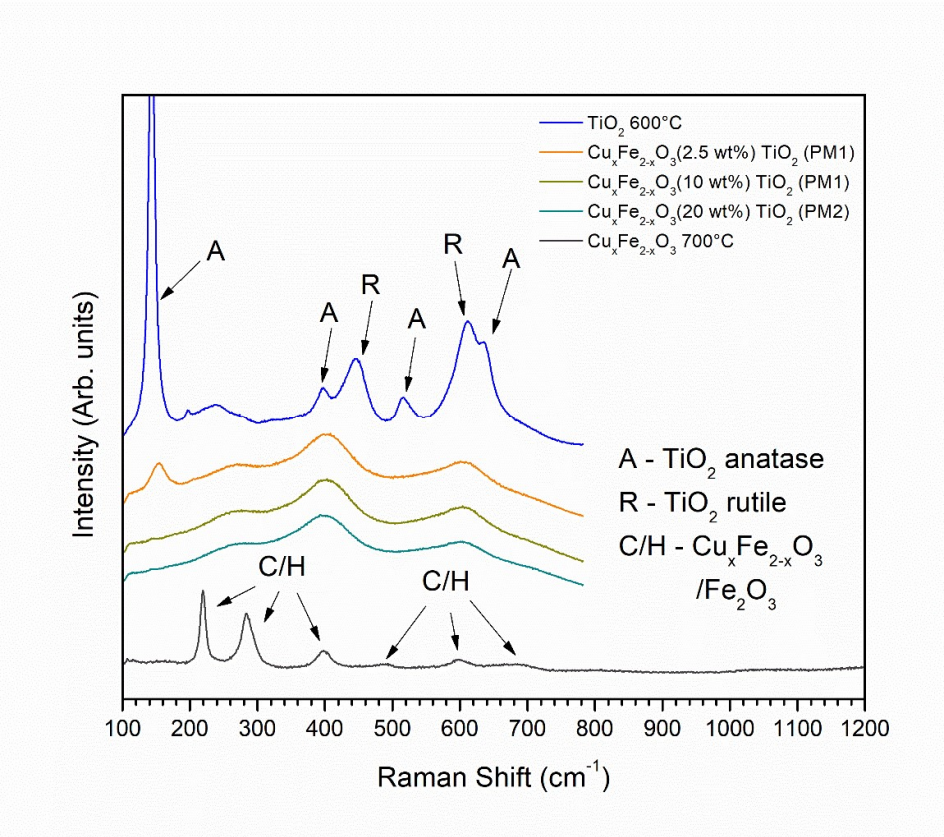

Figure 12. The Raman spectra of TiO_2 600 °C, $Cu_xFe_{2-x}O_3$ (20 wt.%) – TiO_2 (PM2), $Cu_xFe_{2-x}O_3$ (10 wt.%) – TiO_2 (PM1), $Cu_xFe_{2-x}O_3$ (2.5 wt.%) – TiO_2 (PM1) and $Cu_xFe_{2-x}O_3$ 700° C. Dashed lines and capital letters present the positions of TiO_2 anatase (A), TiO_2 rutile (R) and $Cu_xFe_{2-x}O_3$ or α-Fe_2O_3 (hematite) bands (C).

Raman spectroscopy was used to analyse phase composition of samples. In the Raman spectrum of TiO_2 600°C, bands were observed at 146 cm^{-1}, 400 cm^{-1}, 450 cm^{-1}, 519 cm^{-1}, 612 cm^{-1} and 638 cm^{-1}. Bands at 144 cm^{-1} (E_g), 399 cm^{-1} (B_{1g}), 513 cm^{-1} (A_{1g}), 519 cm^{-1} (B_{1g}) and 640 cm^{-1} (E_g) are related to anatase phase (Ohsaka, Izumi und Fujiki 1978) and bans at

447 cm^{-1} (E_g) and 612 cm^{-1} (A_{1g}) are related to rutile phase (Arsov, Kormann und Plieth 1991). Slight difference of band positions could be due to uncertainty of measurements.

The sample $Cu_xFe_{2-x}O_3$ (2.5 wt.%) – TiO_2 (PM1) composed of anatase and rutile, bands were observed at 149 cm^{-1} (anatase) and at 612 cm^{-1} (rutile) as seen from Raman spectra. The samples $Cu_xFe_{2-x}O_3$ (20 wt.%) – TiO_2 (PM2) and $Cu_xFe_{2-x}O_3$ (10 wt.%) – TiO_2 (PM1) were composed of rutile.

Interpretating the phase detection of $Cu_xFe_{2-x}O_3$ was more complicated. $Cu_xFe_{2-x}O_3$ 700°C had Raman bans at 219 cm^{-1}, 283 cm^{-1}, 397 cm^{-1}, 491 cm^{-1}, 600 cm^{-1} and 700 cm^{-1} (**Figure 12**). Bands at 219 cm^{-1}, 283 cm^{-1}, 397 cm^{-1}, 491 cm^{-1} can be related to Fe_2O_3 (Schwaminger, et al. 2017) and/or $Cu_xFe_{2-x}O_3$ (Yadav 2016). The wide band at 700 cm^{-1} can be related to magnemite (Schwaminger, et al. 2017). It could be that tetragonal copper ferrite is also present which has following Raman shifts, 222 cm^{-1}, 288 cm^{-1}, 482 cm^{-1}, 550 cm^{-1}, 607 cm^{-1}, and 691 cm^{-1} , as observed previously in copper ferrite annealed at 1100°C (Yadav 2016).

All samples $Cu_xFe_{2-x}O_3$ (20 wt.%) – TiO_2 (PM2), $Cu_xFe_{2-x}O_3$ (10 wt.%) – TiO_2 (PM1) and $Cu_xFe_{2-x}O_3$ (2.5 wt.%) – TiO_2 (PM1) have wide Raman bands at 260 cm^{-1}, 405 cm^{-1} and 600 cm^{-1}. The Raman bands at 405 cm^{-1} and 600 cm^{-1} overlap with TiO_2 Raman bands at 400 cm^{-1} and 612 cm^{-1}. However, the wide Raman band at 260 cm^{-1} does not correspond to CuO, Fe_2O_3 or $CuFe_2O_4$ (Gan, et al. 2004). The phase composition needs further investigations.

The results of the SEM imaging are presented next.

The SEM images of the pure materials show small grains in TiO_2 600°C (**Figure 13 a**) and larger particles with edges in the $Cu_xFe_{2-x}O_3$ 700°C (**Figure 13 c**). Visually, it can be observed that the SEM images of $Cu_xFe_{2-x}O_3$ (20 wt.%) – TiO_2 (PM2) (**Figure 13 b**) show the formation of larger grains.

From these images the relation between the TiO_2 and $Cu_xFe_{2-x}O_3$ particles in the mixture can be described as the smaller titania particles adhering to the larger synthesised cupper ferrite particles. $Cu_xFe_{2-x}O_3$ works as substrate for TiO_2.

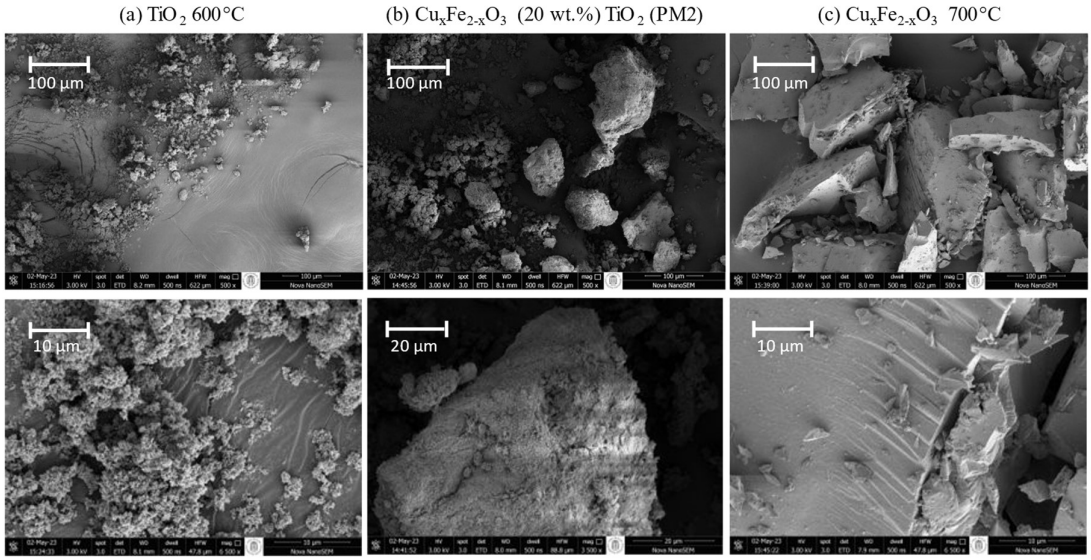

Figure 13. SEM images of **(a)** TiO_2 600°C, **(b)** $Cu_xFe_{2-x}O_3$ (20 wt.%) – TiO_2 (PM2) and **(c)** $Cu_xFe_{2-x}O_3$ 700°C. Each sample has images with two different magnifications. The closer magnification of (b) is one step smaller than of (a) and (c).

As last material characterisation this thesis looks at the absorption spectra of the different materials using diffuse reflection.

The pure white TiO_2 powder start to absorb light below 405 nm. It has main absorbance band at about 325 nm. It correlates well with previously measured absorbance spectra of TiO_2 (P25) (Wang, et al. 2012).

The absorption spectra $Cu_xFe_{2-x}O_3$ annealed at 500°C and 700°C was black and absorption most of the visible light. Previously very high absorbance of $CuFe_2O_4$ in UVA and visible region has been observed (Meidanichil and Ansari 2021).

$Cu_xFe_{2-x}O_3$ (20 wt.%) – TiO_2 (PM2) absorption edge is shifted toward to visible light (absorption edge below 420 nm), depicted as the cyane on **Figure 6.** It has weak absorption band at about 560 nm and at 340 nm. The shift of absorption edge occurs by Cu^{2+} in $Cu_xFe_{2-x}O$ or it could be that there is formation of CuO (Luna, et al. 2016). The weak absorption at 560 nm is related to Fe^{3+} in $Cu_xFe_{2-x}O$ or Fe_2O_3 (Kavitha, et al. 2022).

$Cu_xFe_{2-x}O_3$ (2.5 wt.%) – TiO_2 (PM1) and $Cu_xFe_{2-x}O_3$ (2.5 wt.%) – TiO_2 + 600 °C (PM1) had very similar absorbance in visible range. These two powders show similar red/orange colours after being prepared (**Figure 5**). Samples show a strong redshift. There are two main absorption edges one below 600 nm and other below 410 nm. The first one (below 600 nm)

is related to α-Fe_2O_3 or Fe^{3+} in $Cu_xFe_{2-x}O$ (Kavitha, et al. 2022) and second one CuO (Luna, et al. 2016).

The prepared powders with $Cu_xFe_{2-x}O_3$ (10 wt.%) – TiO_2 (PM1) had three absorption bands at 370 nm, 450 nm and 500 nm in UV-Vis region. These are related to Cu^{2+} in $Cu_xFe_{2-x}O$ or CuO which couples with TiO_2 and absorbance due to Fe^{3+} in $Cu_xFe_{2-x}O$ or γ-Fe_2O_3 (Luna, et al. 2016).

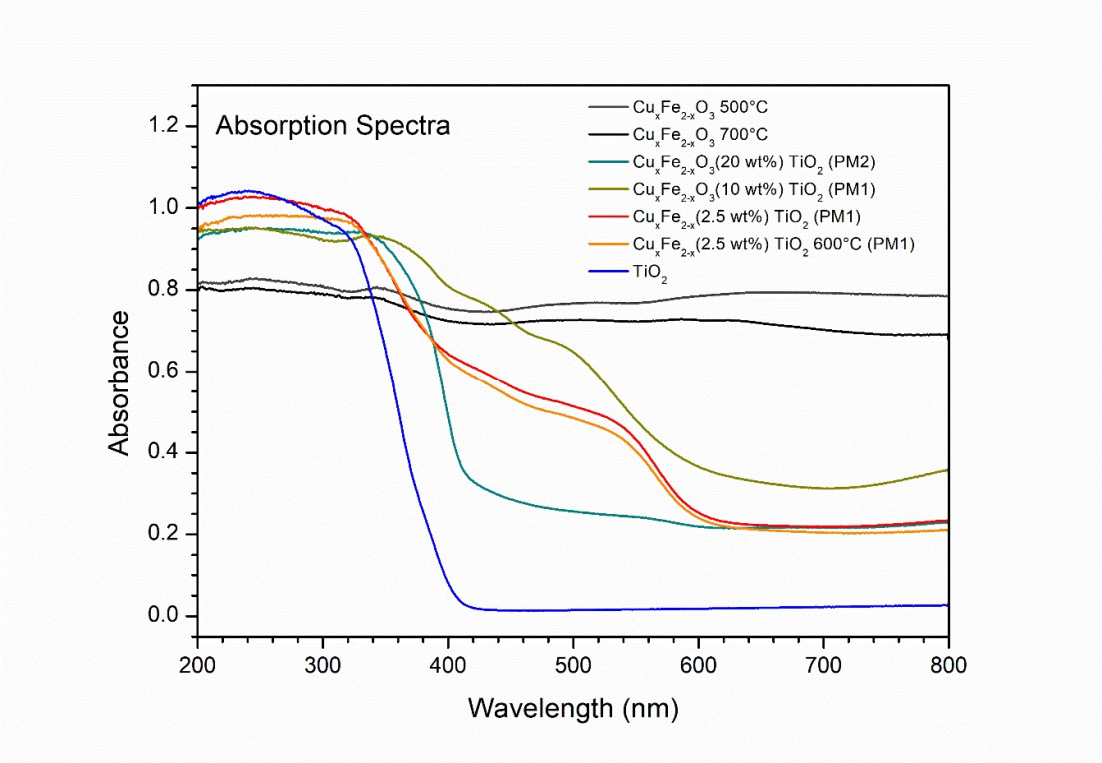

Figure 14. The UV-Vis absorption spectra of pure $Cu_xFe_{2-x}O_3$ annealed at 500 °C and 700°C, $Cu_xFe_{2-x}O_3$ (20 wt.%) – TiO_2 (PM2), $Cu_xFe_{2-x}O_3$ (10 wt.%) – TiO_2 (PM1), $Cu_xFe_{2-x}O_3$ (2.5 wt.%) – TiO_2 (PM1), $Cu_xFe_{2-x}O_3$ (2.5 wt.%) – TiO_2 + 600 °C (PM1) and pure TiO_2.

3.3.2 Degradation of MB with photocatalyst under UVA and visible light

In this section, the photocatalytic evaluation with MB is shown and discussed. The photo-degradation curves are obtained by measuring intensity of MB absorbance band at characteristic wavelength of 665 nm.

First, we will start with the evaluation under UVA radiation.

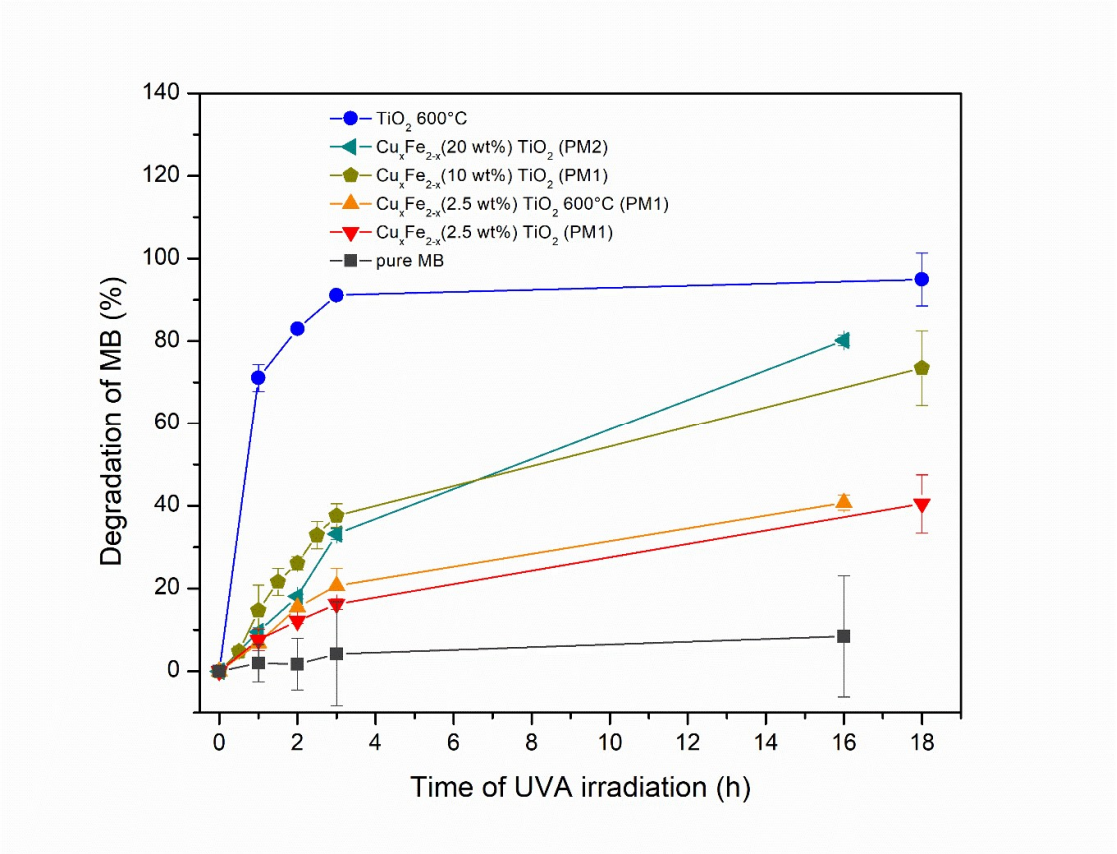

Figure 15. Photocatalytic degradation of MB in solution over time under UVA irradiation by various catalytic powders: $Cu_xFe_{2-x}O_3$ (20 wt.%) – TiO_2 (PM2), $Cu_xFe_{2-x}O_3$ (10 wt.%) – TiO_2 (PM1), $Cu_xFe_{2-x}O_3$ (2.5 wt.%) – TiO_2 (PM1), $Cu_xFe_{2-x}O_3$ (2.5 wt.%) – TiO_2 + 600 °C (PM1) and pure TiO_2 annealed at 650°C. In addition, the degradation of a pure MB aqueous solution is shown.

In **Figure 15** the photodegradation of MB with different catalytic powders is shown. For the pure MB solution, it illustrates that almost no photolysis of pure MB is taken place under UVA and it is photostable. With the various prepared powders, the catalytic activity increasing in the following order: $Cu_xFe_{2-x}O_3$ (2.5 wt.%) – TiO_2 of both preparations < $Cu_xFe_{2-x}O_3$ (10 wt.%) – TiO_2 (PM1) < $Cu_xFe_{2-x}O_3$ (20 wt.%) – TiO_2 (PM2). The reference sample TiO_2 600°C shows the highest photocatalytic activity, even after a short time (3 h). In case of synthesized samples highest activity was detected from $Cu_xFe_{2-x}O_3$ (20 wt.%) – TiO_2 (PM2) with 4 h we reach 38 % MB degradation.

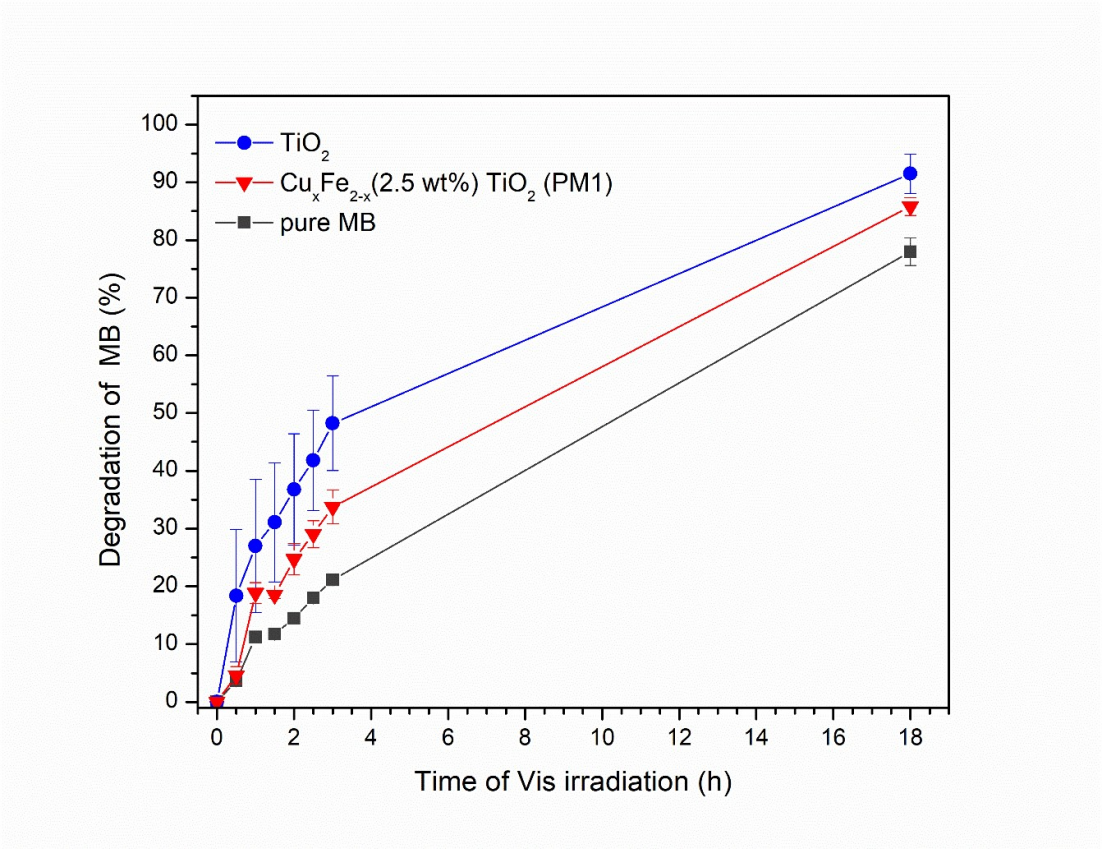

Figure 16. Photocatalytic degradation of MB in solution over time under visible light by various catalytic powders: $Cu_xFe_{2-x}O_3$ (2.5 wt.%) – TiO_2 (PM1) and TiO_2 600°C. In addition, the degradation of a pure MB aqueous solution is shown.

Figure 16 demonstrates the photodegradation of MB with pure TiO_2 and $Cu_xFe_{2-x}O_3$ (2.5 wt.%) – TiO_2 (PM1) under visible light. It illustrates that the MB solution without any catalytic powder shows degradation under the used LED visible light and therefore is not photostable. The solutions with the catalytical powders show higher photocatalytic effect in following increasing order: $Cu_xFe_{2-x}O_3$ (2.5 wt.%) – TiO_2 (PM1) < TiO_2.

This shows a correlation of increasing photocatalytic behaviour with increasing percentage of TiO_2. We explain activity of TiO_2 under visible light due to emittance spectra of LED visible light. It has emittance also below 400 nm. Also, TiO_2 solved so much in water that solution was not transparent.

3.3.3 Degradation of 2,4-D with photocatalyst under UVA

In this section the results of the catalytical powder in relation to the herbicide 2,4-D are shown and discussed.

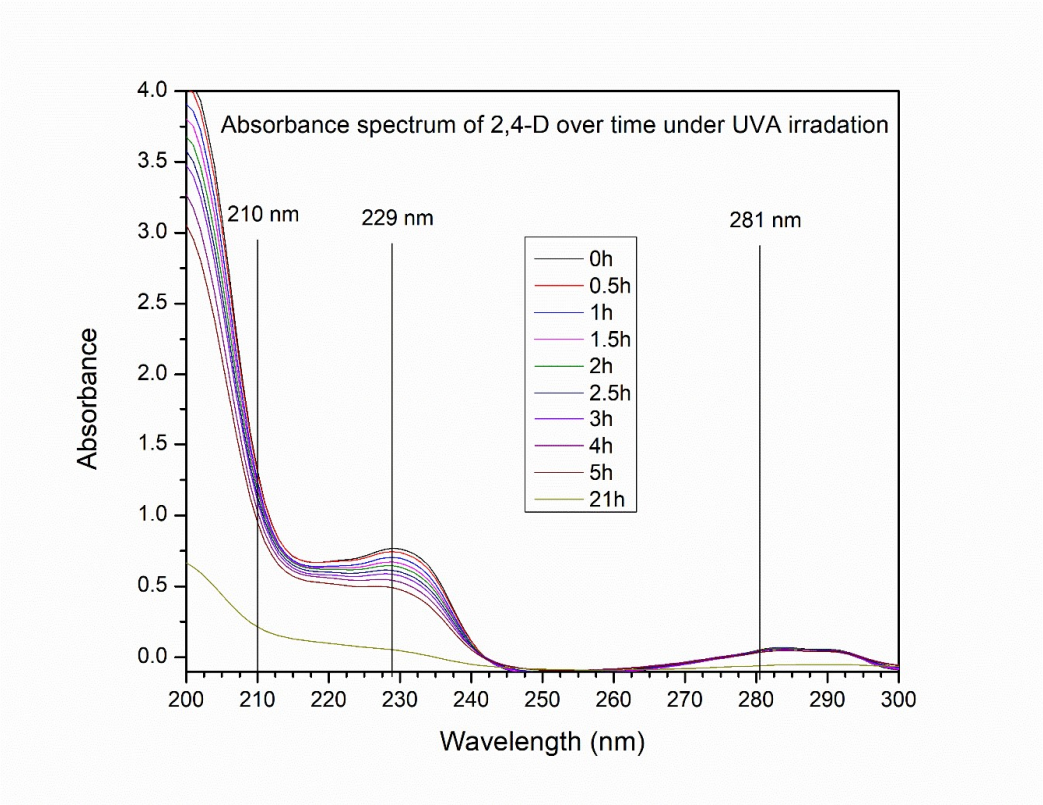

Figure 17. Absorbance spectra of 2,4-D in a solution with the catalytic powder of $Cu_xFe_{2-x}O_3$ (20 wt.%) – TiO_2 (PM2) at different times under UVA irradiation. The vertical lines show characteristic wavelength for 2,4-D.

In **Figure 17** the absorbance spectra of 2,4-D are illustrated at different points during photodegradation on of $Cu_xFe_{2-x}O_3$ (20 wt.%) – TiO_2 (PM2). There are 3 absorption bands which can be seen around 210 nm, 229 nm and 281 nm. Over time all these bands decrease as visible in **Figure 17**.

As already seen in **Figure 1**, 2,4-D is an aromatic compound with two chlorides and one oxyacetic acid group. This makes the aromatic ring conjugated. From literature [(Feigenbrugel, Le Calvé und Mirabel 2006) (Kundu, Pal und Dikshit 2005)] there are two absorption bands associated with the $\pi \rightarrow \pi^*$ transition in the conjugation between 220 nm and 290 nm. The third of our visible absorption band at around 210 nm can be associated within the carboxylic acid group (Koivusalmi 2001).

As 2,4-D shows a characteristic absorption band with the centre of 229 nm, the photodegradation curves of all catalytic powders in **Figure 18** are obtained by measuring decrease of its intensity.

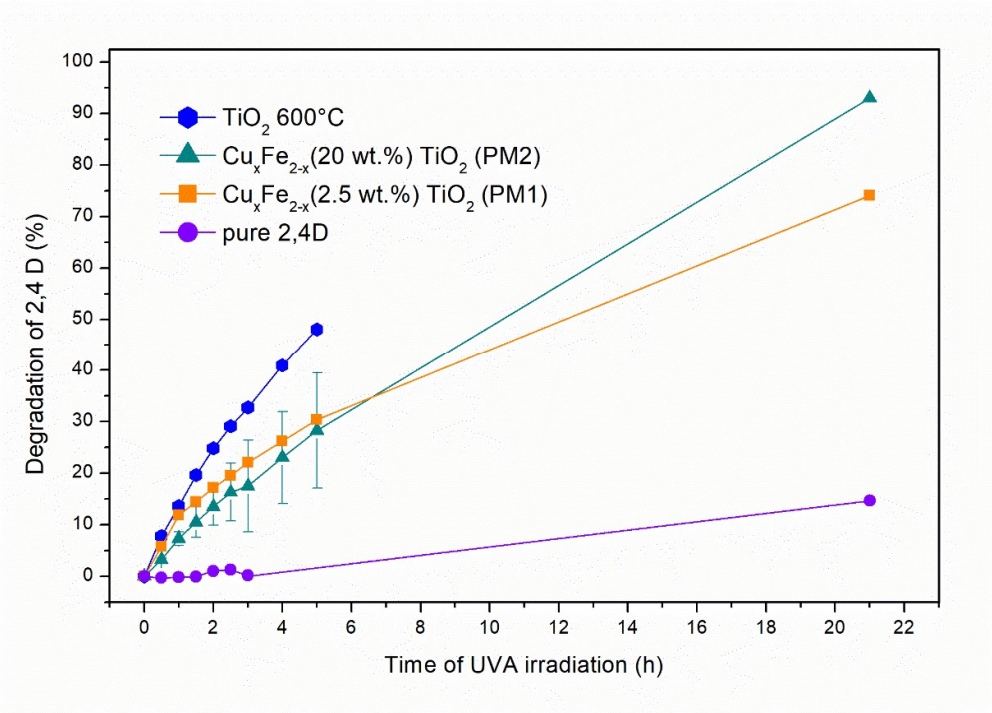

Figure 18. Photocatalytic degradation of 2,4-D in aqueous solution over time under UVA irradiation by various catalytical powders: $Cu_xFe_{2-x}O_3$ (20 wt.%) – TiO_2 (PM2), $Cu_xFe_{2-x}O_3$ (2.5 wt.%) – TiO_2 (PM1) and TiO_2 600°C. In addition, the degradation of a pure 2,4-D aqueous solution is shown.

In **Figure 18** the photodegradation of the 2,4-D in solution with different catalytic powders is shown. For the pure 2,4-D solution, it illustrates that some photolysis is taken place, but in comparison to the solution with the catalytic powders it is less (about 15 % 2,4-D photodegraded under UVA over 24h). After 1 h TiO2 600 °C and $Cu_xFe_{2-x}O_3$ (2.5 wt.%) – TiO_2 (PM1) showed similar efficiency (~12.5 % 2,4-D degradation). After 5 hours of UVA irradiation, it is shown that the at 600 °C annealed pure TiO_2 has the highest photocatalytic effect (50 % of 2,4-D degradation). It can be assumed that the degradation after 21 hours is close to 100% as it had similar photodegradation of MB under UVA irradiation (**Figure 15**). The two prepared powders of $Cu_xFe_{2-x}O_3$ (20 wt.%) – TiO_2 (PM2) and $Cu_xFe_{2-x}O_3$ (2.5 wt.%) – TiO_2 (PM1) show differences in this effect only after leaving the solutions overnight under UVA irradiation, where the powder of higher $Cu_xFe_{2-x}O_3$ amount and (PM2) shows a higher photocatalytic effect on 2,4-D.

On the first look, the catalytical effect of TiO_2 600 °C is faster to degrade MB compared to the herbicide 2,4-D. This does not exclude however that the powder works with the same efficiency over a longer period of UVA irradiation.

In use of our prepared powder $Cu_xFe_{2-x}O_3$ (2.5 wt.%) – TiO_2 (PM1) shows higher degradation of 2,4-D compared with the MB solution under UVA irradiation. The catalytic powder $Cu_xFe_{2-x}O_3$ (20 wt.%) – TiO_2 (PM2) shows a similar photocatalytic effect in both solutions.

The higher photocatalytic activity of pure TiO_2 is related to its high anatase content. Our best performing powder $Cu_xFe_{2-x}O_3$ (20 wt.%) – TiO_2 (PM2) had rutile structure. Also, since the main photoactive material is TiO_2 we had it less on the surface compared to pure TiO_2. $Cu_xFe_{2-x}O_3$ has a density of 5.4 g/cm^3 but TiO_2 anatase only 3.78 g/cm^3 thus we had less photocatalytic material.

3.3.4 Magnetic properties of prepared powders

In **Figure 19** the (a) pure synthesised $Cu_xFe_{2-x}O_3$ annealed at 700°C and the prepared sample (b) $Cu_xFe_{2-x}O_3$ (20 wt.%) – TiO_2 (PM2) are shown when in contact with a magnet. The almost black pure $Cu_xFe_{2-x}O_3$ has very strong magnetic properties as known in literature (Yadav 2016). The synthesized grey powder $Cu_xFe_{2-x}O_3$ (20 wt.%) – TiO_2 (PM2) is also manipulated by the magnet. We also were able to recover the powder from solution after 2,4-D photodegradation. This makes possible to remove this prepared powder from an aqueous solution.

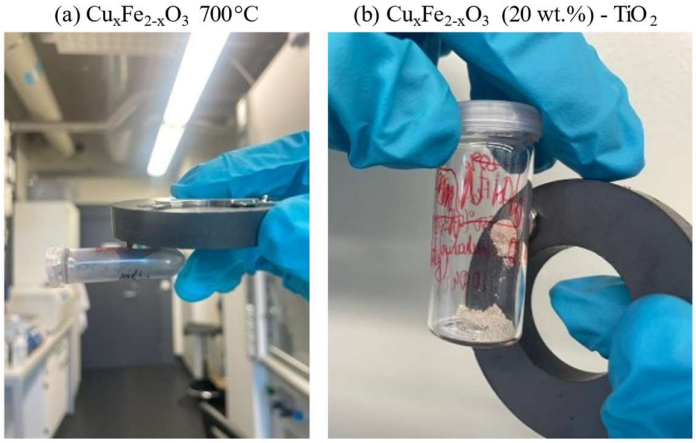

Figure 19. (a) pure $Cu_xFe_{2-x}O_3$ annealed at 700 °C and (b) $Cu_xFe_{2-x}O_3$ (20 wt.%) - TiO_2 in contact with Nd magnet.

SUMMARY

The goal of this thesis was to prepare a photocatalyst that has enhanced properties in comparison to TiO_2 to be used in the treatment of pesticides, like 2,4-D, in wastewater.

Firstly, two simple preparation methods were introduced to make $Cu_xFe_{2-x}O_3$- TiO_2 powders. Both methods included coprecipitation of $Cu_xFe_{2-x}O_3$ by ammonia hydroxide. The attachment of TiO_2 to $Cu_xFe_{2-x}O_3$ was done by either wet or dry method which both involved annealing at high temperatures. As reference pure synthesized $Cu_xFe_{2-x}O_3$ and TiO_2 P25 were used.

A variety of experimental techniques were used to characterize the synthesized samples: XPS for chemical state and surface atomic concentration, NEXAFS for elemental chemical state and local structure, Raman spectroscopy for characterisation of phases, SEM for imaging, UV-Vis for light absorption and photocatalytic evaluation.

The preparation of the samples and the pure synthesized $Cu_xFe_{2-x}O_3$ were relatively pure as the surface atomic concentration shows. According to the studies of XPS and NEXAFS Cu can be found as Cu^{2+} on the surface and Cu^{1+} under it. Fe can be found as Fe^{3+} and Ti as Ti^{4+} under and on the surface.

The wet preparation of $Cu_xFe_{2-x}O_3$ (2.5 wt.%) - TiO_2 shows titania of anatase and rutile structure and the mechanically prepared powder $Cu_xFe_{2-x}O_3$ (20 wt.%) - TiO_2 is composed of rutile on the surface which can be determined by Raman spectroscopy. Additional annealing can be one reasoning behind it.

By using Raman spectroscopy, it was not possible to determine phase composition of the synthesized samples, since $CuFe_2O_4$ Raman bands overlapped with Fe_2O_3. However, it can be presumed based on Raman spectroscopy and NEXAFS spectroscopy that nonmagnetic but photocatalytic sample $Cu_xFe_{2-x}O_3$ (2.5 wt.%) – TiO_2 (PM1) was composed of CuO and α-Fe_2O_3 (hematite) mixture or with some $CuFe_2O_4$. The magnetic sample $Cu_xFe_{2-x}O_3$ (20 wt.%) – TiO_2 (PM2) is composed of CuO and γ-Fe_2O_3 (maghemite) mixture or $CuFe_2O_4$.

According to SEM analysis annealed TiO_2 has fine structure but $Cu_xFe_{2-x}O_3$ has particle size up to 100 μm. Thus $Cu_xFe_{2-x}O_3$ works as substrate for TiO_2. Huge particles make it easy to capture the photocatalytic material.

With the help of UV-vis absorbance spectroscopy, it is shown that the synthesized samples have a shifted absorption edge toward to visible light. This is related to Cu^{2+} and Fe^{3+} in the structure of $Cu_xFe_{2-x}O$ or formed separate CuO or Fe_2O_3. Since $Cu_xFe_{2-x}O_3$ (20 wt.%) - TiO_2,

prepared with the dry method, was magnetic it is assumed that it consist of $Cu_xFe_{2-x}O$ or γ-Fe_2O_3.

Next, the photocatalytic activity was proven in all prepared mixtures of TiO_2 and our synthesized material. For example, $Cu_xFe_{2-x}O_3$ (20 wt.%) - TiO_2 (PM2) degraded about 38% of MB and 15% of 2,4-D after 3 hours. After UVA irradiation overnight, the mechanically prepared powder degraded 95% of 2,4-D and $Cu_xFe_{2-x}O_3$ (2.5 wt.%) - TiO_2 (PM1) degraded 70% of 2,4-D in solution. Under visible light $Cu_xFe_{2-x}O_3$ (2.5 wt.%) - TiO_2 (PM1) was photocatalytic.

Our better performing sample $Cu_xFe_{2-x}O_3$ (20 wt.%) - TiO_2 was composed of TiO_2 rutile, and $Cu_xFe_{2-x}O$ or γ-Fe_2O_3. Rutile is known as less photocatalytic than anatase. Also, if the main photoactive material is TiO_2 there was less of it in measurement compared to pure TiO_2, since $Cu_xFe_{2-x}O_3$ has higher density (5.4 g/cm^3) than TiO_2 anatase (3.78 g/cm^3).

Lastly, another goal was to synthesize photocatalytic powder which can easily be captured from solutions like wastewater tanks. This was achieved by creating $Cu_xFe_{2-x}O_3$ (20 wt.%) - TiO_2. This preparation enables TiO_2, our main photoactive material, to be attached to a larger particle (in microns), which in addition inhibits magnetic properties.

Future work on the material $Cu_xFe_{2-x}O_3$ - TiO_2 should be focused on XRD and other studies for the determination of phase composition. In addition, the photocatalytic activity under visible light in a 2,4-D solution should be conducted, as photolysis under visible light can be an important feature used in wastewater treatments.

REFERENCES

ACS. *ACS - Molecule of the week.* 27 08 2012. https://www.acs.org/molecule-of-the-week/archive/d/24-dichlorophenoxyacetic-acid.html (accessed 05 16, 2023).

an der Laan, G., C. Westra, C. Haas, and G. A. Sawatzky. "Satellite structure in photoelectron and Auger spectra of copper dihalides." *Physical Review B* 23 (1981): 4369.

Anadan, S., Y. Ikuma, and K. Niwa. "An Overview of Semi-Conductor Photocatalysis: Modification of TiO2 Nanomaterials." *Solid State Phenomena* 162 (2010): 239-260.

Arsov, Lj. D., C. Kormann, and W. Plieth. "Electrochemical synthesis and in situ Raman spectroscopy of thin films of titanium dioxide." *Journal Raman Spectroscopy* 22 (1991): 573.

Belessiotis, George V., Pinelopi P. Falara, Islam Ibrahim, and Athanassios G. Kontos. "Magnetic Metal Oxide-Based Photocatalysts with Integrated Silver for Water Treatment." *Materials* 15 (2022): 4629.

Fairley, Neal, et al. "Systematic and collaborative approach to problem solving using X-ray photoelectron spectroscopy." *Applied Surface Science Advances* 5 (2021): 100112.

Feigenbrugel, Valérie, Stéphane Le Calvé, and Philippe Mirabel. "Molar absorptivities of 2,4-D, cymoxanil, fenpropidin, isoproturon and pyrimethanil in aqueous solution in the near-UV." *Spectrochimica Acta Part A: Molecular and Biomolecular Spectroscopy* 63 (2006): 103-110.

Fujishima, Akira, Xintong Zhang, and Donald A. Tryk. "TiO2 photocatalysis and related surface phenomena." *Surface Science Reports* 63 (2008): 515-582.

Gaffard, Agathe, Olivier Pays, Karine Monceau, Maria Teixeira, Vincent Bretagnolle, and Jérôme Moreau. "Feeding on grains containing pesticide residues is detrimental to offspring development through parental effects in grey partridge." *Environmental Pollution* 312 (2022): 120005.

Gan, Z. H., G. Q. Yu, B. K. Tay, C. M. Tan, Z. W. Zhao, and Y. Q. Fu. "Preparation and characterization of copper oxide thin films deposited by filtered cathodic vacuum arc." *Journal of Physics D, Applied Physics* 37 (2004): 81-85.

Garvie, Laj, AJ Craven, and R Brydson. "Use of Electron-Energy-Loss Near-Edge Fine-Structure in the Study of Minerals." *American Mineralogist* 79, no. 5-6 (1994): 411-425.

Grioni, M., et al. “Studies of copper calence states with Cu L3 x-ray-absorption spectroscopy.” *Physical Review B* 39 (1989): 1541-1545.

Janczarek, Marcin, and Ewa Kowalska. “On the Origin of Enhanced Photocatalytic Activity of Copper-Modified Titania in the Oxidative Reaction Systems.” *Catalyst* 7 (2017): 317.

Kavitha, S., et al. “Fabrication of visible-light-responsive TiO2/α-Fe2O3-heterostructured composite for rapid photo-oxidation of organic pollutants in water.” *Journal of Materials Science: Materials in Electronics* 33 (2022): 8906-8919.

Koivusalmi, Eija. *Characterisation and analysis of synthesis mixtures of hydroxy aldehydes, hydroxy carboxylic acids and polyols.* Academic Dissertation, Helsinki: University of Helsinki, Department of Chemistry, 2001.

Kundu, Sanghamitra, Anjali Pal, and Anil K. Dikshit. “UV induced degradation of herbicide 2,4-D: kinetics, mechanism and.” *Separation and Purification Technology* 44 (2005): 121-129.

Lashgari, M. “In Micro and Nano Technologies, Nanomaterials for CO2 Capture, Storage, Conversion and Utilization.” In *Fundamental aspects of CO2 transformation into C/H/O based fuels/chemicals*, by M. Lashgari, edited by P. N. Tri, H. Wu, T. A. Nguyen, S. Barnabe, & P. Benard, 283-305. Amsterdam: Elsevier, 2021.

Lee, H., et al. “Photocatalytic reactions of 2,4-dichlorophenoxyacetic acid using a microwave-assisted photocatalysis system.” *Chemical Engineering Journal* 278 (2015): 259-264.

Luna, A. L., et al. “Photocatalytic degradation of gallic acid over CuO-TiO2 composites under UV/Vis LEDs irradiation.” *Applied Catalysis A: General* 521 (2016): 140-148.

Marlina, Emy, Sze Nee Goh, Ta Yeong Wu, Tongling Tan, Sharifah Bee Abd Hamid, and Joon Ching Juan. “Evaluation on the Photocatalytic Degradation Activity of Reactive Blue 4 using Pure Anatase Nano-TiO2.” *Sains Malaysiana* 44, no. 7 (2015): 1011-1019.

McCafferty, E. P., and J. Wightman. “Determination of the concentration of surface hydroxyl groups on metal oxide films by a quantitative XPS method.” *Surface Interface Analysis* 26 (1998): 549-564.

Meidanichil, Alireza, and Hoorieh Ansari. “Copper Spinel Ferrite Superparamagnetic Nanoparticles as a Novel Radiotherapy Enhancer Effect in Cancer Treatment.” *Journal of Cluster Science* 32 (2021): 657-663.

Michelin, A., E. Drouet, E. Foy, J.J. Dynes, D. Neffa, and P. Dillmann. “Investigation at the nanometre scale on the corrosion mechanisms of archaeological ferrous artefacts by STXM .” *Journal of Analytical Atomic Spectrometry* 28 (2013): 59-66.

Moulder, John F., William F. Stickle, Peter E. Sobol, and Kenneth D. Bomben. *Handbook of X-ray Photoelectron Spectroscopy.* Eden Prairie: Perkim-Elmer Corporation, 1992.

Müeller. *Photoelectron spectrometer, ESCALAB Mk II by Vacuum Generators.* 2017. https://jacobs.physik.uni-saarland.de/home/index.php?page=steinbeiss/home_cms_steinbeissdet3-1&navi=service (accessed 05 20, 2023).

Ohsaka, Toshiaki, Fujio Izumi, and Yoshinori Fujiki. “Raman spectrum of anatase, TiO2.” *Journal of Raman Spectroscopy* 71 (1978): 97-106.

Pawestri, Imelda Nafa, and Erma Sulistyaningsih. “Neurobehavioral perfomance of Indonesioan farmers and its association with pesticides exposure: A cross-sectional study.” *Clinical Epidemiology and Global Health* 11 (2021): 100754.

Saleh, Iman A., Nabil Zouari, and Mohammed A. Al-Ghouti. “Removal of pesticides from water and wastewater: Chemical, physical and biological treatment approaches.” *Environmental Technology & Innovation* 19 (2020): 101026.

Sayed, Akram, Michael Chys, Jasmine De Rop, Liliane Goeteyn, Pieter Spanoghe, and Imca Sampers. “Pesticide residue in (treated) wastewater and products of Belgian vegetable- and potato processing companies.” *Chemosphere* 280 (2021): 130619.

Schwaminger, Sebastian, et al. “Bio-nano interactions: Cellulase on iron oxide nanoparticle surfaces.” *Adsorption* 23 (2017): 281-292.

Seah, M. P., Ian S. Gilmore, and S. J. Spencer. “Quantitative XPS.” *Journal of Electron Spectroscopy and Related Phenomina* 120 (2001): 93-111.

Sharma, Anket, et al. “Worldwide pesticides usage and its impact on ecosystem.” *Springer Nature Applied Sciences* 1 (2019): 1446.

Shaw, Duncan J. *Introduction to Colloid and Surface Chemistry.* Oxford: Butterworth-Heinemann, 1992.

Stöhr, J. *NEXAFS spectroscopy.* Berlin: Springler-Verlag, 1992.

Syafrudin, M., et al. “Pesticides in Drinking Water A Review.” *Int. J. Environ. Res. Public Health* 18 (2021): 468.

Wang, Xiaoling, Simo O. Pehkonen, Jaakko Rämö, Marja Väänänen, James G. Highfield, and Kari Laasonen. “Experimental and computational studies of nitrogen doped Degussa P25 TiO2: application to visible-light driven photo-oxidation of As(iii).” *Catalysis Science and Technology* 2 (2012): 784-793.

Watts, John F., and John Wolstenholme. *An Introduction to Surface Analysis by XPS and AES.* Chichester: Wiley, 2003.

Xu, Z., et al. “Recent Developments on Gas-Phase Volatile Organic Compunds Abatement on Photocatalysis.” *Adv. Energy Sustainability Res.* 3 (2022): 2200105.

Yadav, Singh. “Cation Migration-Induced Crystal Phase Transformation in Copper Ferrite Nanoparticles and Their Magnetic Property.” *Raghvendra J Supercond Nov Magn* 29 (2016): 759-769.

NON-EXCLUSIVE LICENCE TO REPRODUCE THESIS AND MAKE THESIS PUBLIC

I, Franziska Maria Bundrück,

1. herewith grant the University of Tartu a free permit (non-exclusive licence) to

reproduce, for the purpose of preservation, including for adding to the DSpace digital archives until the expiry of the term of copyright,

Photocatalytic degradation of 2,4-Dichlorophenoxyacetic acid by $Cu_xFe_{2-x}O_3$,

supervised by Dmytro Danilian and Rainer Pärna.

2. I grant the University of Tartu a permit to make the work specified in p. 1 available to the public via the web environment of the University of Tartu, including via the DSpace digital archives, under the Creative Commons licence CC BY NC ND 3.0, which allows, by giving appropriate credit to the author, to reproduce, distribute the work and communicate it to the public, and prohibits the creation of derivative works and any commercial use of the work until the expiry of the term of copyright.

3. I am aware of the fact that the author retains the rights specified in p. 1 and 2.

4. I certify that granting the non-exclusive licence does not infringe other persons' intellectual property rights or rights arising from the personal data protection legislation.

Franziska M. Bundrück

23/05/2023